Chemical Geology 584 (2021) 120507

Contents lists available at ScienceDirect

Chemical Geology

journal homepage: www.elsevier.com/locate/chemgeo

Quartz chemistry of granitic pegmatites: Implications for classification, genesis and exploration

Axel Müller [a,b,*], William Keyser [a], William B. Simmons [c], Karen Webber [c], Michael Wise [d], Hartmut Beurlen [e], Idoia Garate-Olave [f], Encarnación Roda-Robles [f], Miguel Ángel Galliski [g]

[a] Natural History Museum, University of Oslo, 0318 Oslo, Norway
[b] Natural History Museum, London, UK
[c] MP2 Research Group, Maine Mineral and Gem Museum, PO Box 500, 99 Main Street, Maine 04217, USA
[d] Department of Mineral Sciences, Smithsonian Institution, Washington, D.C 20560, USA
[e] Federal University of Pernambuco, Department of Geology, Recife, Brazil
[f] Dpto. Geología, Univ. País Vasco-UPV/EHU, Barrio Sarriena s/n, 48940 Leioa, Spain
[g] IANIGLA, CCT-MENDOZA CONICET, Av. Ruiz Leal s/n, Parque Gral. San Martín, C.C. 330 (5.500) Mendoza, Argentina

ARTICLE INFO

Editor: Karen Johannesson

Keywords:
Quartz
Pegmatite
Lithium
Trace elements
LA-ICP-MS

ABSTRACT

Quartz from 254 pegmatites representing eight pegmatite fields and provinces worldwide was investigated by laser-ablation inductively-coupled plasma mass spectrometry (LA-ICP-MS) to determine concentrations of trace elements Al, Ti, Li, Ge, B, Be, Rb, Na, K, Ca, P, Ga, Sb, Zn and U. A total of 271 new analyses combined with 535 published LA-ICP-MS quartz chemistry data were evaluated with binary and ternary trace element discrimination plots and principal component analysis (PCA). The classifications applied for discrimination of pegmatite types include the widely applied NYF(Nb-Y-F) - LCT(Li-Cs-Ta) classification and the new RMG (pegmatites derived from residual melts of granite magmatism) - DPA (pegmatites as direct products of anatexis) grouping. Pegmatites of both classifications can be well distinguished via Al-Ti, Al-Li and Al/Ti-Ge/Ti binary trace element plots and the Ti - Al/10 - 10*Ge ternary diagram. PCA applied to Al, Li, Ti, Be, B, Ge and Rb contents in quartz allowed to further distinguish between anatectic DPA-1 (Li-enriched DPA) and granite-pluton-derived RMG-1 (Li-enriched RMG) pegmatites. Some pegmatite fields and provinces (Hagendorf-Pleystein, Oxford County) are distinguishable by region-specific Li, Ge and Al contents. The results imply that the chemistry of pegmatite quartz is mainly controlled by the origin (source rock chemistry) of pegmatite melts and, to a much lesser extent, by the geodynamic setting of the pegmatite fields and provinces. Chemically primitive NYF and DPA-2 type pegmatites contain quartz with the lowest total trace-element contents and lowest internal-pegmatite trace-element variation, making it potentially suitable for high-tech application. Pegmatite quartz containing >30 $\mu g g^{-1}$ Li and >100 $\mu g g^{-1}$ Al is strongly indicative of economic spodumene/montebrasite mineralization and, thus, serves as a strong Li-mineralization pathfinder mineral. Quartz with >5 $\mu g g^{-1}$ B may be a potential indicator for gem-quality tourmaline mineralization.

1. Introduction

Quartz comprises 20 to 40% of granitic pegmatites, typically displaying large crystal dimensions, making it a major mineral constituent of these rocks and an important economic resource. The high resistance of quartz to alteration compared to, for example, feldspars and micas, makes it a reliable mineral to study fractionation and crystallization processes and the nature of melt over protracted geological histories. Ironically, quartz is the least studied of the important minerals in pegmatites.

Trace elements of rock-forming minerals are considered important petrogenetic indicators for determining the P-T-X conditions of mineral formation, for obtaining information about fluid or melt origin and for discriminating different crystallization environments. Quartz incorporates only a few elements at very low concentrations owing to the fact that a limited number of ions can substitute for Si^{4+} in the quartz crystal lattice, mainly Al, Ge, Ti, P, B and Fe^{3+} (Weil, 1984, 1993; Götze et al., 2004; Müller and Koch-Müller, 2009), or can enter interstitial

* Corresponding author.
E-mail address: a.b.mueller@nhm.uio.no (A. Müller).

https://doi.org/10.1016/j.chemgeo.2021.120507
Received 9 July 2021; Received in revised form 18 August 2021; Accepted 25 August 2021
Available online 27 August 2021

lattice positions, mainly H, Li, Na, K, Fe^{2+} and Be (Bambauer, 1961; Kats, 1962; Perny et al., 1992; Stalder et al., 2017; Potrafke et al., 2019). Aluminum is the most abundant ion in quartz (up to a few thousand $\mu g g^{-1}$) because of its common availability and similar ionic radius to Si^{4+}. Trace elements in lesser concentrations in quartz are Ga, Sn, Sr, Rb, Mn and Sb (Walenczak, 1969; Larsen et al., 2000; Rusk et al., 2011; Monnier et al., 2021). Other elements commonly identified by mass spectrometry in quartz, such as Ca, Mg, Ba, REE, U and Th, are attributable to microinclusions of fluids or other minerals (Gerler, 1990; Blankenburg et al., 1994; Götze et al., 2004; Götze, 2009).

The number of studies of quartz chemical composition has increased in recent years owing to instrumental developments in laser-based mass spectrometry (LA-ICP-MS), allowing for *in situ* analysis of mineral trace elements at concentrations of $<1\ \mu g g^{-1}$ (Larsen et al., 2000, 2004; Götze et al., 2005; Müller et al., 2008, 2015; Breiter et al., 2014, 2019; Garate-Olave et al., 2017; Hong et al., 2021; Maneta and Baker, 2019; Ashworth et al., 2020). These studies, and the results from FTIR spectrometry (Müller and Koch-Müller, 2009; Stalder et al., 2017; Stalder, 2021; Potrafke et al., 2019), have found Al, Ge, Ti, P, B, H, Li, Na, K, Rb and Be to be the main trace elements found in pegmatite quartz. The concentrations of these elements are used for geographic or genetic discrimination or to establish crystallization conditions. Parameters controlling the uptake into the quartz lattice are well established for some of these trace elements, e.g., Ti concentrations in quartz increase with increasing temperature (Wark and Watson, 2006) and pressure (Huang and Audétat, 2012). Germanium, Rb, B and Be concentrations in quartz increase with the fractionation degree of the melt (Larsen et al., 2000; Jacamon and Larsen, 2009; Müller et al., 2015, 2018). Parameters controlling the uptake of Al and Li in the lattice of pegmatite quartz are, however, still debated (e.g., Müller and Koch-Müller, 2009). In experimental studies, Frigo et al. (2016) observed that the abundance of LiOH defects in quartz increases with increasing Li saturation, temperature and pressure in granitic melt systems. At pressures >15 kbar and temperatures >600°C, however, no LiOH defects were detected in synthetic quartz. Based on a large dataset of quartz trace element chemistry from granitic rocks, Breiter et al. (2020) suggested that Al contents of quartz above $450\ \mu g g^{-1}$ indicate an S-type affinity of the granite host, while Al contents $<250\ \mu g g^{-1}$ are typical for A-type granitic rocks.

Černý (1991) introduced the benchmark geochemical subdivision of rare-element pegmatites into the Nb-Y-F (NYF), Li-Cs-Ta (LCT) and mixed NYF-LCT families, which is today widely used. The family classification implies that LCT pegmatites are related to S-type granitic magmas found in orogenic settings, whereas NYF pegmatites are derived from late- to post-tectonic to anorogenic A-type granites. As attractive as this straightforward classification appears, the simple fact is that all too frequently the tectonic setting of the parent granite (if identified) is unknown (Wise, 2013) and distinguishing between genetic families of NYF and LCT pegmatites is complex. In a new pegmatite classification attempt, Wise et al. (2021) utilized a more comprehensive suite of accessory minerals to define six pegmatite groups, which are genetically related to either granite plutons or the anatexis of metaigneous and metasedimentary protoliths. Pegmatites belonging to the first two groups are generated from the residual melts of S-, A- and I-type granite magmatism (RMG-1, RMG-2 and RMG-1+2, respectively; Table 1). The population of RMG-1 pegmatites related to fertile S-type granites is characterized by enrichment in Li, Rb, Cs, Be, Sn, Nb, Ta, B, P and F. The geochemical signature of RMG-2 pegmatites derived from fertile A-type granites is characterized by high abundances of Ga, Zr, Y, Nb, Ti, U, Th, REEs, Zn, F and Cl. RMG-1+2 pegmatites have an overall chemistry similar to I-type granites with enrichments of B, Be, REE, Nb, Ti, Li and Ca. The other three groups are direct products of anatexis of metamorphic rocks. Depending on the chemical signature of the partial melts having either S-, A- or I-type affinity, Wise et al. (2021) further distinguished these groups as DPA-1 (enriched in Be, Nb, Ta, P, Li), DPA-2 (enriched in REE, U, Be) and DPA-3 (enriched in Al, Be, B), respectively. In this study, we test if quartz chemistry can be used to distinguish between the LCT and NYF pegmatite families as defined by Černý (1991) and the RMG and DPA group classification of Wise et al. (2021). The subgroups DPA-3, RMG-2 and RMG-1+2 are, however, not represented in this study.

In this study we evaluate and compare new and published datasets comprising 806 LA-ICP-MS analyses of trace element concentrations in quartz from 254 pegmatites from eight pegmatite fields and provinces worldwide (Table 1). The mineralogy, geochemistry, geological setting and crystallization age of the studied pegmatites vary over a wide range. Of the 806 quartz analyses evaluated in this study, 535 were previously published (Müller et al., 2008, 2015; Beurlen et al., 2011; Dill et al., 2013; Garate-Olave et al., 2017), while the remaining 271 analyses are new data (Table 2). The aim is to test the applicability of quartz trace-element chemistry to distinguish between different pegmatite types and its potential as a pathfinder for pegmatites with Li, Ta, Nb and REE mineralization. Additionally, we discuss the parameters controlling the uptake of Al, Ge, Ti, P, B, H, Li, Na, K, Rb and Be in the quartz lattice and how these elements can be used to better understand the origin and crystallization of pegmatite melts.

Table 1
General characteristics of RMG and DPA type pegmatites according Wise et al. (2021).

RMG (Residual melts of granite magmatism)			
Petrogenetic type - mineralogical group	RMG - Group 1	RMG - Group 2	RMG - Group 1+2
Typical source rock	S-type granites	A-type granites	I-type granites
Granite chemistry	Peraluminous	Peralkaline & metaluminous to mildly peraluminous	Peraluminous to metaluminous
Relation of pegmatites to source	Interior to marginal	Interior to marginal	Interior to marginal
Typical geochemical signatures	Be, Nb, Ta, P, Sn, Li, Cs	REE, Be, Nb, F	B, Be, REE, Nb, Ti, Li, Ca
DPA (Direct products of anatexis)			
Petrogenetic type - mineralogical group	DPA - Group 1	DPA - Group 2	DPA - Group 3
Typical source rock	Granulite to amphibolite facies metasediments and metaigneous rocks of granitic S-type signature	Granulite to amphibolite facies F-rich amphibolites and metaigneous rocks of granitic A-type signature	Granulite to amphibolite facies metagraywackes and metaigneous Al-rich rocks
Relation of pegmatites to source	Segregations of anatectic melts	Segregations of anatectic melts	Segregations of anatectic melts
Typical geochemical signatures	Be, Nb, Ta, P, Li	REE, U, Be	Al, Be, B

Table 2
Major characteristics of the sampled pegmatite fields and provinces. For references of pegmatite crystallization ages see text. NYF – Nb-Y-F pegmatite family; LCT - Li-Cs-Ta pegmatite family; RMG – pegmatites being product of Residual Melts of Granite magmatism; DPA – pegmatite melts being Direct Products of Anatexis.

Pegmatite field or province	Pegmatite province	Country	Age (Ma)	Orogen	Pegmatite subclass (Černý and Ercit, 2005)	Pegmatite family (Černý, 1991)	Pegmatite group (Wise et al., 2021)	Number of sampled pegmatites	Number of quartz analyses	Origin of quartz data set
Evje-Iveland	South Scandinavian	Norway	896- 924	Sveconorwegian	Muscovite rare-element REE and rare-element REE	NYF	DPA-2	96	218	Müller et al. (2015)
Froland	South Scandinavian	Norway	1090–1060	Sveconorwegian	Abyssal HREE, muscovite rare-element REE and rare-element REE	NYF	DPA-2	91	161	Müller et al. (2008, 2015)
Tørdal	South Scandinavian	Norway	884-907	Sveconorwegian	Muscovite rare-element REE and rare-element REE	NYF	DPA-2	36	160	This study
Borborema	Borborema	Brazil	509- 525	Brasiliano/ Pan-African	Rare-element Li	LCT	DPA-1	5	72	Beurlen et al. (2011)
Tres Arroyos	Iberian	Spain	307-309	Variscan	Rare-element Li	LCT	RMG-1	5	54	Garate-Olave et al. (2017)
Pleystein-Hagendorf	Pleystein-Hagendorf	Germany	295-299	Variscan	Rare-element Li	LCT	RMG-1	5	30+11	Dill et al. (2013) and this study
San Luis	Pampean	Argentina	440-460	Famatinian	Rare-element Li	LCT	DPA-1	8	30	This study
Oxford County	Oxford County	USA	270-250	Alleghenian	Rare-element Li	LCT	DPA-1	8	70	This study

2. Description of the studied pegmatite fields and provinces

2.1. Evje-Iveland pegmatite field, Norway

The Evje-Iveland field is located in southern Norway ~50 km N of Kristiansand and comprises approximately 400 major pegmatite occurrences. The field belongs to the Sveconorwegian Setesdal pegmatite district as part of the South Scandinavian pegmatite province. The pegmatites are mainly hosted by banded amphibolitic gneisses, gabbroic amphibolites and metadiorites as part of the Sveconorwegian Rogaland-Hardangervidda-Telemark Sector. Major minerals within the pegmatites include K-feldspar, plagioclase, quartz, biotite and muscovite with minor magnetite and garnet. Common accessory minerals are beryl, gadolinite-(Y), allanite-(Ce), monazite-(Ce), fergusonite-(Y), euxenite-(Y), xenotime-(Y), zircon, rutile, ilmenite and thortveitite (Andersen, 1931; Barth, 1931, 1947; Bjørlykke, 1934, 1937; Müller et al., 2012a). The pegmatites are well-zoned with a granitic wall facies, a megacrystic intermediate zone and a core of massive quartz. Some of the evolved pegmatites exhibit albite replacement zones that, in addition to the main minerals albite and muscovite, also contain topaz, fluorite, columbite group minerals, spessartine, beryl, quartz and schorl (Frigstad, 1999). The pegmatites belong to the rare-element REE and muscovite rare-element REE class with NYF affinity according to the classification of Černý (1991) and Černý and Ercit (2005). Uranium-Pb ages of gadolinite-(Y) (Scherer et al., 2001), monazite-(Y) (Ling et al., 2017; Seydoux-Guillaume et al., 2012) and columbite group minerals (Müller et al., 2017) range from 896 to 924 Ma. The Høvringsvatnet granite pluton north of the pegmatite field has a crystallization age of 976 to 987 Ma (U-Pb zircon; Snook, 2014) and is genetically unrelated to the pegmatite formation (Müller et al., 2015). Field observations, geochemical modelling and the age difference between the granite and pegmatites provide evidence for formation of the Evje-Iveland pegmatites by partial melting of the amphibolitic host rocks (Snook, 2014; Müller et al., 2015, 2017). The quartz chemistry dataset used here was previously published by Müller et al. (2015).

2.2. Froland pegmatite field, Norway

The Froland pegmatite field comprises more than 105 large (>1,000 m^3) pegmatite bodies, which occur within a NNE-SSW-trending area measuring 20 by 5 km (Müller et al., 2008, 2015). The pegmatite field, which lies above the SE-dipping basal thrust of the Porsgrunn-Kristiansand fault zone, is oriented roughly parallel to the fault. The multigenerational Froland field is subdivided into synorogenic- (1090-1060 Ma), late orogenic- (926 ± 8 Ma reported as the emplacement age of the nearby Herefoss pluton and Holtebu granite; Andersen, 1997) and postorogenic pegmatites (<926 ± 8 Ma; Ihlen et al., 2002; Müller et al., 2008). In this study, only synorogenic pegmatites, which constitute more than 95% of the pegmatite bodies in the field, are considered. The pegmatites form large tabular bodies and dykes that are either unzoned or show a simple mineralogical zoning. They were emplaced within an isoclinally folded sequence of steeply-dipping banded biotite-hornblende gneisses of volcano-sedimentary origin being part of the Sveconorwegian Bamble Sector (Cosca et al., 1998; Henderson and Ihlen, 2004; Bingen et al., 2008; Nijland et al., 2014). Major minerals of the pegmatites are quartz, K-feldspar, plagioclase, biotite and subordinate white mica (Ihlen et al., 2001, 2002). Although the pegmatites are generally very low in garnet and accessory Y-REE-Nb-Th minerals, some groups of pegmatites show enhanced contents of NYF-type rare-mineral assemblages including, for example, euxenite-(Y), samarskite-(Y), aeschynite-(Y), fergusonite-(Y), allanite-(Ce), thorite, and uraninite (Andersen, 1926, 1931; Bjørlykke, 1937; Ihlen et al., 2001, 2002; Larsen, 2002; Larsen et al., 2004; Müller et al., 2008, 2012a). According to the classification of Černý and Ercit (2005), the synorogenic Froland pegmatites comprise simple abyssal, primitive rare-element REE and muscovite rare-element REE pegmatites. Primitive rare-element pegmatites refer to pegmatites containing dark mica as the only mica species, low-Rb K-feldspar and very few REE minerals. The emplacement

ages of these pegmatites range from 1030 to 1090 Ma (Rosing-Schow et al., 2021) and are thus significantly older than the nearby Herefoss pluton and Holtebu granite. According to Müller et al. (2008), melts forming the Froland synorogenic pegmatites were generated by fluid-present crustal melting in zones of localized high-strain deformation during progressive thrusting along the Porsgrunn-Kristiansand fault zone. The Froland quartz datasets utilized in this study are taken from Müller et al. (2008, 2015).

2.3. Tørdal pegmatite field, Norway

The Tørdal pegmatite field is part of the South Scandinavian pegmatite province and comprises more than 300 large-scale (>1000 m^3) pegmatites. The pegmatites are hosted by amphibolites of the supracrustal Nissedal outlier as part of the Sveconorwegian Rogaland-Hardangervidda-Telemark Sector in southern Norway (Oftedal, 1940; Bergstøl and Juve, 1988). Major minerals of the pegmatites include K-feldspar, quartz, plagioclase, biotite, muscovite and albite (Rosing-Schow et al., 2018). Common accessory minerals are garnet, gadolinite-(Y), monazite-(Ce), allanite-(Ce) and molybdenite. The most evolved pegmatites additionally contain accessory polylithionite-trilithionite, polylithionite-siderophyllite, columbite group minerals, topaz, fluorite, cassiterite and beryl (Bergstøl and Juve, 1988; Rosing-Schow et al., 2018). The evolved pegmatites show zonation with discordant albite replacement zones close to the core. The pegmatites are classified as rare-element REE and muscovite rare-element REE types with chemical NYF signature. Uranium-Pb dating of ixiolite and monazite-(Ce) revealed pegmatite crystallization ages of 892.7 ± 8.8 Ma and 905.0 ± 2.4 Ma, respectively (Rosing-Schow et al., 2021). The Tørdal granite pluton, located south of the pegmatite field, has an emplacement age of 946 ± 4 Ma (U-Pb zircon and Nb-Y-oxide; Rosing-Schow et al., 2021). Based on field evidence and pegmatite and granite ages, Rosing-Schow et al. (2021) suggested that the Tørdal pegmatite melts were formed directly by melting of amphibolitic host rocks. In this study, a new quartz trace-element dataset is provided, comprising 160 quartz analyses from 36 different pegmatites.

2.4. Borborema pegmatite province, NE Brazil

The Borborema pegmatite province extends over an area of approximately 75 x 150 km in the states of Paraíba and Rio Grande do Norte in northeast Brazil. There are over 700 Be-Li-Ta mineralized pegmatite bodies in the area, occurring along the eastern part of the Seridó Belt in the northern Borborema tectonic province (Brito Neves and Fuck, 2013). The pegmatites are hosted by Neoproterozoic supracrustal metasedimentary rocks of the Seridó Group, which consists mainly of garnet-cordierite-sillimanite-biotite gneisses and schists, quartzites, meta-arkoses, metaconglomerates and calc-silicate gneisses with some marble and orthoamphibolite intercalations (Van Schmus et al., 2003). Main minerals of the pegmatites comprise K-feldspar, plagioclase, quartz and muscovite, with abundant black and rare colored tourmaline, including blue Paraíba tourmaline. Characteristic accessory minerals are beryl, garnet, columbite group minerals, cassiterite, spodumene, lepidolite and gahnite. The pegmatites show a distinct internal zoning and are classified as the rare-element Li type of the LCT family (Beurlen et al., 2014). Some of the evolved bodies belong to the complex-spodumene or -lepidolite subtype according to the classification of Černý and Ercit (2005). Pegmatite crystallization ages range from 509 to 525 Ma (Araújo et al., 2005; Baumgartner et al., 2006; Beurlen et al., 2009). The pegmatites are associated with several pegmatitic granite intrusions with a crystallization age of 520 ± 10 Ma (Pb/U/Th uraninite and xenotime; Beurlen et al., 2014).

2.5. Tres Arroyos pegmatite field, Spain

The Late-Variscan Tres Arroyos granite-pegmatite field is located at the southwest margin of the Central Iberian Zone of the Variscan Massif, approximately 10 km NW of the town of Alburquerque in western Spain (Garate-Olave et al., 2017). The field is about 3 km long and 1 km wide and occurs along the southwestern contact of the Nisa-Alburquerque batholith. The batholith consists mainly of porphyritic peraluminous monzogranite and a minor two-mica leucogranitic facies (Gallego-Garrido, 1992; González-Menéndez, 1998). The emplacement age of the monzogranite is 305-309 Ma (U-Pb SHRIMP and LA-ICP-MS of zircon; Solá et al., 2009). The pegmatites, with a crystallization age of 305 ± 9 Ma (U-Pb columbite group minerals), are interpreted to be fractionated residual melts of the Nisa-Alburquerque batholith (Garate-Olave et al., 2020). Both granites and pegmatites intruded Precambrian phyllites, slates, schists, quartzites and metagreywackes. Barren, intermediate and evolved aplite-pegmatite bodies occur in the area (Gallego-Garrido, 1992; Garate-Olave et al., 2017, 2020). The barren layered aplite-pegmatites, which outcrop close to the Nisa-Alburquerque batholith, comprise about 15 bodies. Besides feldspars and quartz, the pegmatites contain mica of the muscovite-zinnwaldite series, topaz, Sn-Ta-Nb oxides and Fe-Mn phosphates. Some of the dykes are only aplitic, whereas in other bodies aplite and pegmatite occur as alternating layers. The intermediate bodies form sub-horizontal, leucocratic aplite-pegmatite dykes up to 8 m in thickness. They are composed of albite and quartz with K-feldspar and micas as major minerals, whereas topaz, Li-Al-phosphates, apatite group minerals and Nb-Ta-Sn-oxides occur as accessory phases. Some of these bodies display a rhythmic banding between alternating albite- and quartz-rich layers. Evolved Li-F-rich aplite-pegmatites occur the farthest away from the batholith. There are approximately twelve Li-F-rich aplite-pegmatites in the area and they contain abundant Li-rich mica, topaz and amblygonite-montebrasite. They typically show layering with alternating Li-micas and quartz + albite-rich zones. Quartz trace-element data used in this study was published by Garate-Olave et al. (2017).

2.6. Hagendorf-Pleystein pegmatite province, Germany

The Variscan Hagendorf-Pleystein pegmatite province is located in the Moldanubian zone (Moldanubicum), the core zone of the central European Variscides, between the towns of Waidhaus and Pleystein in Oberpfalz, southeast Germany. The field comprises three major stock-like bodies, the Hagendorf-South, Hagendorf-North and Pleystein pegmatites, the stockscheider-type pegmatite at Silbergrube and numerous small aplitic-pegmatitic bodies, all enriched in Li, Nb and P (Strunz et al., 1975; Müller et al., 1998; Dill et al., 2007, 2009; Dill, 2015). The enrichment of P provides a variable association of phosphate minerals (Gruß, 1950; Strunz, 1957; Mücke, 1981). The stock-like bodies are zoned with a muscovite-albite wall zone, an intermediate, eutectic quartz-feldspar zone, a blocky feldspar zone and a massive quartz core. Major minerals are quartz, K-feldspar, plagioclase, albite and muscovite and common accessories include columbite group minerals, apatite, zwieselite, triphylite, fluorite, autunite, torbernite, bismuth and sulphides. The pegmatites are classified as rare-element Li pegmatites of the LCT family. The host rocks comprise mainly high-temperature/low-pressure paragneisses, which are intercalated with quartzites, calc-silicate rocks, amphibolites and metagabbros. According to Siebel et al. (1995), the pegmatites crystallized from residual melts of the phosphorus-rich Křížový kámen/Kreuzstein granite (297±2 Ma; Siebel et al., 1995). For this study, the four major pegmatites of Hagendorf-South, Hagendorf-North, Pleystein and Silbergrube were sampled. Some of the quartz trace-element data was previously published by Dill et al. (2012).

2.7. San Luis pegmatite district, Argentina

The eight Argentinian pegmatites sampled for this study occur in three fields of the San Luis pegmatite district and include the Totoral, Conlara and La Estanzuela fields (Table 2). The district is part of the

Pampean pegmatite province, which extends more than 800 km N-S and 200 km E-W, mostly in the Sierras Pampeanas of northwestern and central Argentina (Galliski, 1992, 1994a, 1994b, 2009). Major pegmatite minerals are quartz, K-feldspar, albite and muscovite and typical accessory minerals include garnet, beryl, 'lepidolite', spodumene, amblygonite-montebrasite, columbite group minerals, pyrochlore and microlite subgroup minerals, Fe-Mn and Al-Li phosphates, rutile and bismuthinite (Galliski and Márquez-Zavalía, 2011). The host rocks comprise Cambrian amphibolite-facies paragneisses, which were deformed at ~450-500°C and 2-4 kbar between 498±10 and 456±19 Ma (Steenken et al., 2006). The pegmatites are classified as orogenic rare-element and muscovite rare-element pegmatites belonging to the petrogenetic family of LCT pegmatites. The pegmatites are of five mineralogical types: (1) barren to transitional to beryl type, (2) beryl-columbite-phosphate subtype of the beryl type, (3) spodumene subtype of the complex type, (4) albite-spodumene type and (5) albite type. Pegmatite age determinations range from 306 to 527 Ma (Linares, 1959; Galliski and Linares, 1999; López de Luchi et al., 2002). Recent dating provided reliable U-Pb columbite ages ranging from 512.6±10 Ma to 412±19 Ma for the orogenic pegmatites and 369.3±3.78 Ma for the post-orogenic La Viquita pegmatite (Von Quadt, 2011; Galliski et al., 2021). Most of the analyzed quartz crystals come from pegmatites that are genetically linked to the Cerro La Torre and Loma Alta – Paso del Rey pegmatitic leucogranites. The favored genetic model for this leucogranite-pegmatite suite is episodic crustal anatexis, produced by muscovite ± biotite dehydration melting of paragneisses by shear-heating during a collisional orogeny (Galliski, 2009; Galliski et al., 2019).

2.8. Oxford County pegmatite field, Maine, USA

The Oxford County pegmatite field comprises about 100 pegmatites distributed over an area of 60 x 40 km in southwestern Maine. The pegmatites are largely hosted by the Sebago Migmatite-Granite Complex with the Sebago pluton in its southern part (Solar and Brown, 2001; Solar and Tomascak, 2009, 2016; Solar et al., 2017; Wise and Brown, 2010). Pegmatites consist of albite, K-feldspar, quartz, muscovite and biotite. Black tourmaline (schorl) and almandine-spessartine garnet are common accessory minerals. Other characteristic accessories are fluorapatite, spodumene, 'lepidolite', pollucite, Al-Li and Fe-Mn phosphates, beryl, cassiterite and columbite group minerals. The pegmatites of the Oxford County pegmatite field belong to the LCT family of rare-element pegmatites. In general, three categories of pegmatites have been recognized: (1) quasi-homogeneous, simple pegmatites, (2) beryl ± columbite ± phosphate-bearing and (3) complex Li-enriched pegmatites (spodumene petalite subtype). Miarolitic cavities hosting gem-quality minerals are uncommon in most Oxford County pegmatites but are best developed in the Li-enriched pegmatites. The migmatites of the Sebago complex formed at 376 ± 14 Ma, whereas the Sebago pluton and other small granite bodies have crystallization ages between 297 ± 14 and 288 ± 13 Ma (U-Pb zircon; Solar and Tomascak, 2016). Uranium-Pb zircon, columbite-tantalite and apatite, and Sm-Nd garnet dating of the pegmatites yielded ages from ~ 270 to 250 Ma, clearly younger than the migmatites and granites (Bradley et al., 2016; Roda-Robles, unpublished data; Tanja Knoll and Ralf Schuster, personal communication in Webber et al., 2019). Webber et al. (2019) proposed an anatectic origin for the Oxford County pegmatites via a process related to decompression melting associated with post-Appalachian unroofing and increased thermal input accompanying the early stages of rifting of Pangea. For this study, the Mt. Mica, Berry-Havey, Bennett, Emmons, Tamminen, Plumbago North, West Hayes Ledge and Orchard pegmatites were sampled and analyzed.

3. Sampling and analytical methods

The majority of investigated quartz samples were taken from the intermediate zones of lens-shaped or dyke-like pegmatite bodies. Five representative pegmatites that include those from Skåremyr in Froland, Steli in Evje-Iveland, Øvre Høydalen in Tørdal, Berry-Havey in Oxford County and Capoeira 2 in Borborema were more extensively sampled by collecting quartz from all zones to investigate the intra-pegmatite variability of quartz chemistry (Fig. 1).

Trace element concentrations in quartz were determined by LA-ICP-MS using a Thermo Instruments double-focusing sector field mass spectrometer model ELEMENT XR based at the Geological Survey of Norway in Trondheim. The instrument is coupled to a New Wave 193-nm excimer laser probe for sample ablation. Both the 271 new analyses and the 535 published analyses included in this study were performed on the same instrument following the same methodology. Laser raster ablation was performed in the center of quartz crystals on an area of approximately 400 × 150 μm using a spot size of 50 μm. The elements analyzed include Li, Be, B, Mn, Ge, Rb, Sr, Na, Al, P, K, Ca, Ti, Fe, Sb, U, Zn and Ga. External calibration was performed using six silicate glass reference materials. The isotope ^{30}Si was used as an internal standard. Ten sequential measurements performed on a synthetic quartz crystal were used to estimate the limits of detection, which were based on 3 x standard deviation (3σ). The detection limits are 5 $\mu g g^{-1}$ for Al, 1 $\mu g g^{-1}$ for Ti, 0.5 $\mu g g^{-1}$ for Li and 0.2 $\mu g g^{-1}$ for Ge. Further details on measurement procedures are described by Flem et al. (2002) and Flem and Müller (2012).

4. Results

4.1. Variability of average quartz trace-element contents among pegmatite fields

Average trace-element concentrations of quartz from the eight investigated pegmatite fields are listed in Table 3. The complete list of performed LA-ICP-MS analyses is provided in the Supplementary Material SMTable 1. Concentrations of Sb, U, Zn and Ga are only available for the Tørdal, Tres Arroyos, Pleystein-Hagendorf, San Luis and Oxford County pegmatite fields and provinces. Most of the values obtained for Sb, U, Zn and Ga, as well as Na, P, K, Ca and Fe, are below the detection limits. Infrequently occurring Na concentration spikes of up to 300 $\mu g g^{-1}$ are attributable to incidental ablation of NaCl-bearing fluid inclusions within quartz. The laser ablation equipment used in this study did, however, allow for high-resolution video control of the analyzed quartz domain to avoid incidental contamination from micro-fluid and mineral inclusions (Flem and Müller, 2012). However, in some quartz samples, in particular those from the San Luis district and the Oxford County field, the abundance of fluid inclusions was very high and in some cases did not allow for complete avoidance of fluid-inclusion-free areas for laser ablation analysis.

The most abundant trace element in quartz in all pegmatite types included in this study is Al followed by Li, Ti, Ge, B, Mn, Be, Rb and Sr (Table 3). The south Norwegian pegmatites, classified as NYF or DPA-2 pegmatites, contain quartz with much lower average Al than that of pegmatites classified as LCT or DPA-1 and RMG-1 (Fig. 2). Quartz from the Hagendorf-Pleystein pegmatites has outstandingly high Al (average 785 $\mu g g^{-1}$) whereas that of Evje-Iveland, Froland and Tørdal NYF/DPA-2 pegmatites has low Al (average 49, 40 and 80 $\mu g g^{-1}$, respectively). The south Norwegian NYF/DPA-2 pegmatite quartz is also typically lower in Li, Ge, B and Rb compared to that of LCT/DPA-1/RMG-1 pegmatites. Among the LCT/DPA-1/RMG-1 pegmatites, quartz from the Hagendorf-Pleystein province has a markedly low average Ge and Li. Quartz from the RMG-1 pegmatites from Tres Arroyos and Hagendorf-Pleystein has the highest average Rb among the investigated pegmatites.

4.2. Variability of quartz trace-element contents within individual pegmatite bodies

Quartz samples were taken along profiles across five pegmatites in

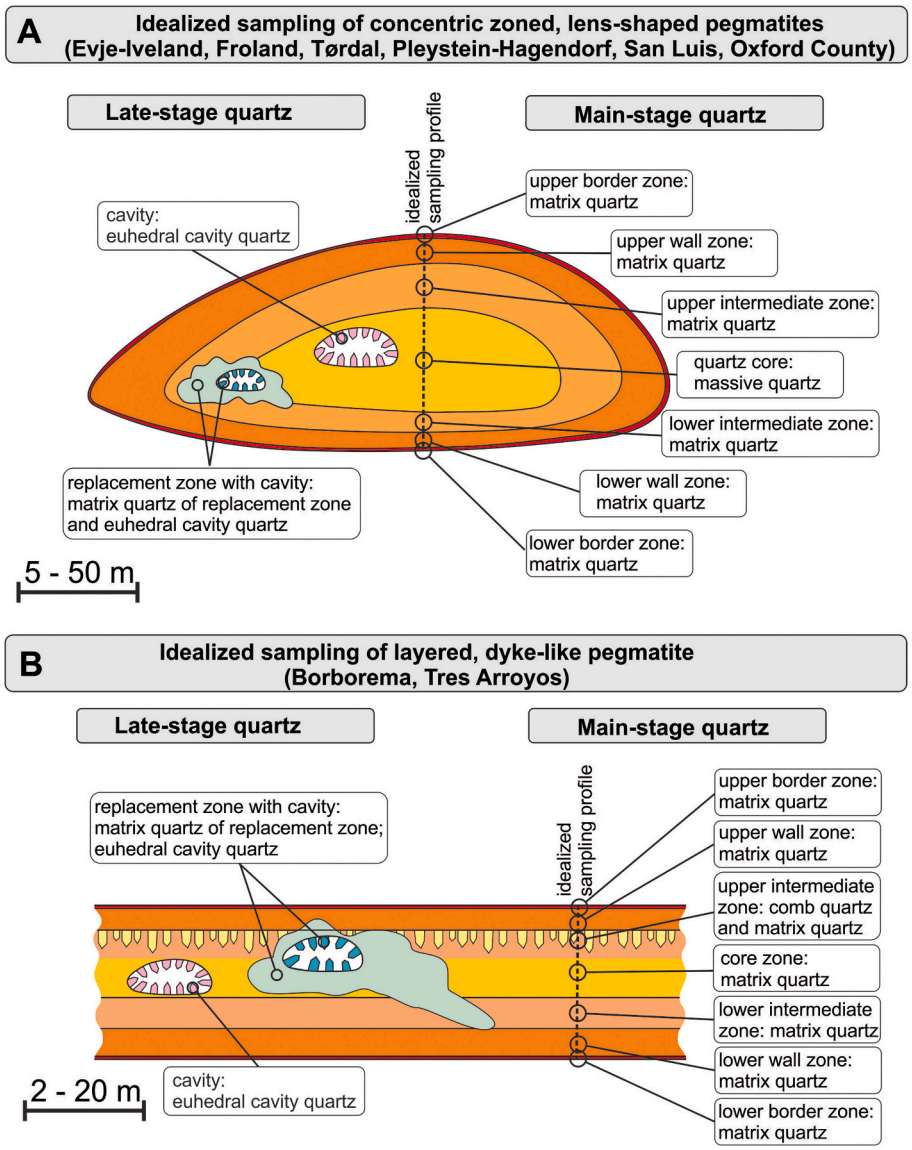

Fig. 1. Quartz sampling approach for (A) zoned lens-shaped pegmatites and (B) dyke-like pegmatites.

order to examine variations of trace-element contents in quartz. The chemically primitive Skåremyr NYF/DPA-2 pegmatite from Froland contains quartz with relatively consistent contents of Li, Ge, Al and Ti throughout its core to wall zones (Fig. 3). Quartz of the moderately evolved NYF/DPA-2 Steli pegmatite from Evje-Iveland shows increasing concentrations of Al and Li from the margin to the core of the pegmatite, from 16 to 36 $\mu g g^{-1}$ and from 8 to 11 $\mu g g^{-1}$, respectively. The Ti content conversely decreases from 13 $\mu g g^{-1}$ in the upper border zone to 5 $\mu g g^{-1}$ in the core zone. The evolved NYF/DPA-2 Øvre Høydalen pegmatite contains quartz showing a different chemical trend, with Li, Al and Ti concentrations decreasing from pegmatite margin to core whereas Ge increases. The Øvre Høydalen quartz chemistry is also unique in that the total trace-element content decreases from margin to core in the pegmatite.

Quartz from the Berry-Havey pegmatite shows a marked decrease in Ti concentration from the border/wall (13.3 $\mu g g^{-1}$) to the core (0.6 $\mu g g^{-1}$) and an increase in Ge from 1.3 to 19.4 $\mu g g^{-1}$, whereas Al and Li behave less distinctly. Quartz of the evolved LCT/DPA-1 Capoeira 2 pegmatite has a very distinct symmetric pattern: Li, Ge and Al increase towards the core while Ti decreases. The total trace-element content of the core quartz is almost 5 times higher than that of the border zone quartz, the most significant pegmatite-internal variation observed so far.

The five quartz chemistry profiles share the characteristic of increasing Ge and decreasing Ti from pegmatite margin to core. Aluminum and Li appear to be paired although they can increase or decrease from pegmatite margin to core. All other trace elements lack noteworthy variations from pegmatite margin to core.

4.3. Variability of quartz chemistry among pegmatite fields illustrated as binary plots

Representative binary plots that highlight trace-element variations in quartz are shown in Fig. 4. The Al versus Ti plot in Fig. 4A discriminates well between regional and genetic pegmatite groups but with overlaps. The separated data clouds of NYF/DPA-2 and LCT/ DPA-1/ RMG-1 pegmatites are the most distinctive. Quartz of the latter is characterized by high (>100 $\mu g g^{-1}$) to very high (up to 4000 $\mu g g^{-1}$) Al compared to the former. Exceptions to the low Al in quartz from NYF/ DPA-2 type pegmatites are a few samples of highly evolved Tørdal and Evje-Iveland pegmatites with quartz containing Al up to 500 $\mu g g^{-1}$. However, the Al threshold of 100 $\mu g g^{-1}$ seems to be a significant marker that might be used as a criterion to distinguish between NYF/DPA-2 and LCT/ DPA-1/RMG-1 pegmatites. Quartz from NYF/DPA-2 pegmatites generally has higher Ti contents than quartz from LCT/ DPA-1/RMG-1

Table 3
Average trace element concentrations of quartz. The "less than" sign in front of average values (AVG) higher than the limit of detection (LOD) indicate that the majority of analyses is below the limit of detection. n.d. - not determined; n - number of analyses.

	Li	Be	B	Mn	Ge	Rb	Sr	Na	Al	P	K	Ca	Ti	Fe	Sb	U	Zn	Ga	total
Evje-Iveland (n = 218)																			
LOD	*0.50*	*0.15*	*0.60*	*0.20*	*0.20*	*0.07*	*0.05*	*6.0*	*5.0*	*3.0*	*5.0*	*8.0*	*1.50*	*1.00*	*n.d.*	*n.d.*	*n.d.*	*n.d.*	
AVG	**6.61**	**0.23**	**0.9**	**0.33**	**2.32**	**0.09**	**<0.05**	**<6.0**	**68.5**	**<3.0**	**<5.0**	**<8.0**	**19.07**	**<1.00**	**n.d.**	**n.d.**	**n.d.**	**n.d.**	**121**
STD	4.15	0.24	0.8	0.38	1.81	0.15	-	13.2	55.3	-	-	-	11.26	-	-	-	-	-	87
Froland (n = 161)																			
LOD	*0.50*	*0.15*	*0.60*	*0.20*	*0.20*	*0.07*	*0.05*	*6.0*	*5.0*	*3.0*	*5.0*	*8.0*	*1.50*	*1.00*	*n.d.*	*n.d.*	*n.d.*	*n.d.*	
AVG	**11.19**	**0.10**	**0.6**	**<0.20**	**1.42**	**0.05**	**<0.07**	**<7.3**	**45.6**	**<3.0**	**<5.0**	**<8.0**	**7.43**	**<1.00**	**n.d.**	**n.d.**	**n.d.**	**n.d.**	**91**
STD	6.85	0.07	0.6	-	0.81	0.09	0.19	28.1	23.2	-	-	-	3.00	-	-	-	-	-	63
Tørdal (n = 160)																			
LOD	*0.07*	*0.03*	*1.67*	*0.02*	*0.21*	*0.03*	*0.02*	*10.5*	*4.9*	*2.0*	*18.0*	*5.6*	*0.84*	*0.62*	*0.01*	*0.01*	*1.15*	*0.03*	
AVG	**20.02**	**0.24**	**1.7**	**0.35**	**4.49**	**0.18**	**0.11**	**<10.5**	**104.6**	**<2.0**	**<18.0**	**<5.6**	**11.67**	**<1.05**	**0.10**	**<0.01**	**<1.38**	**<0.05**	**182**
STD	10.05	0.47	1.2	0.49	4.09	0.62	0.46	-	101.4	-	-	-	7.29	2.75	0.10	-	0.95	0.07	130
Borborema (n = 72)																			
LOD	*0.30*	*0.08*	*1.10*	*0.14*	*0.04*	*0.03*	*0.02*	*16.2*	*5.4*	*3.2*	*2.9*	*14.1*	*0.90*	*0.53*	*n.d.*	*n.d.*	*n.d.*	*n.d.*	
AVG	**56.34**	**0.42**	**3.6**	**0.62**	**5.34**	**0.05**	**0.04**	**<16.2**	**264.8**	**<3.2**	**<2.9**	**<14.1**	**9.87**	**<0.53**	**n.d.**	**n.d.**	**n.d.**	**n.d.**	**378**
STD	45.62	0.26	3.4	3.77	5.44	0.09	0.04	-	180.4	-	-	-	6.50	-	-	-	-	-	246
Tres Arroyos (n = 54)																			
LOD	*0.07*	*0.03*	*1.67*	*0.02*	*0.21*	*0.03*	*0.02*	*10.5*	*4.9*	*2.0*	*18.0*	*5.6*	*0.84*	*0.62*	*0.01*	*0.01*	*1.15*	0.03	
AVG	**56.96**	**0.17**	**3.1**	**0.28**	**4.14**	**4.45**	**0.07**	**<16.4**	**371.8**	**<9.3**	**<14.6**	**<5.6**	**2.65**	**<0.62**	**0.22**	**<0.01**	**<1.15**	**<0.08**	**492**
STD	31.41	0.12	2.0	0.15	1.15	9.39	0.03	42.0	223.5	3.8	17.2	-	2.66	-	0.48	-	-	0.07	334
Hagendorf-Pleystein (n = 41)																			
LOD	*0.07*	*0.03*	*1.67*	*0.02*	*0.21*	*0.03*	*0.02*	*10.5*	*4.9*	*2.0*	*18.0*	*5.6*	*0.84*	*0.62*	*0.01*	*0.01*	*1.15*	*0.03*	
AVG	**16.95**	**0.44**	**5.9**	**0.96**	**2.14**	**3.96**	**0.41**	**<10.5**	**1055.8**	**<4.9**	**301.5**	**<5.6**	**7.46**	**17.04**	**<0.01**	**<0.01**	**<1.15**	**<0.03**	**1435**
STD	9.28	0.25	4.4	1.32	0.65	7.05	1.33	-	880.7	5.0	509.0	-	3.53	33.32	-	-	-	-	1456
San Luis (n = 30)																			
LOD	*0.07*	*0.03*	*1.67*	*0.02*	*0.21*	*0.03*	*0.02*	*10.5*	*4.9*	*2.0*	*18.0*	*5.6*	*0.84*	*0.62*	*0.01*	*0.01*	*1.15*	*0.03*	
AVG	**45.23**	**0.30**	**3.5**	**0.59**	**9.10**	**1.47**	**0.07**	**<34.1**	**412.4**	**<2.0**	**<95.2**	**<5.6**	**2.42**	**<1.14**	**<0.01**	**<0.01**	**<1.15**	**<0.03**	**614**
STD	48.82	0.27	2.2	1.07	4.34	2.53	0.09	64.6	405.3	-	146.7	-	1.94	1.82	-	-	-	-	680
Oxford County (n = 70)																			
LOD	*0.07*	*0.03*	*1.67*	*0.02*	*0.21*	*0.03*	*0.02*	*10.5*	*4.9*	*2.0*	*18.0*	*5.6*	*0.84*	*0.62*	*0.01*	*0.01*	*1.15*	*0.03*	
AVG	**76.47**	**0.43**	**8.6**	**2.42**	**7.49**	**0.11**	**<0.02**	**<35.8**	**352.4**	**<2.0**	**<18.0**	**<5.6**	**3.60**	**<4.29**	**0.34**	**0.43**	**<2.54**	**<0.11**	**521**
STD	79.10	0.93	21.8	17.81	7.67	0.31	-	156.5	335.6	-	-	-	5.38	17.93	1.62	2.42	3.18	0.22	650

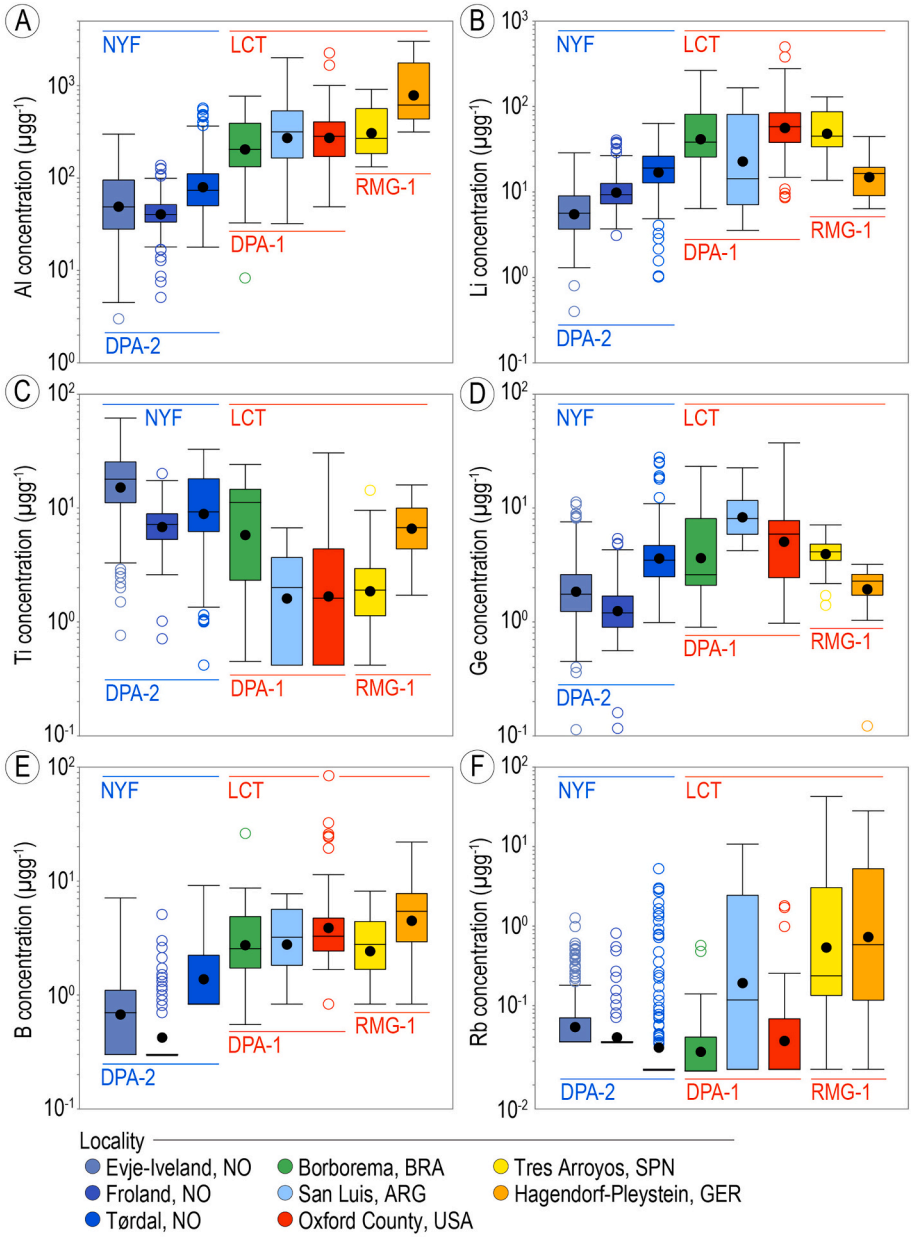

Fig. 2. Box-and-whisker diagrams showing the range of (A) Al, (B) Li, (C) Ti, (D) Ge, (E) B and (F) Rb concentrations in quartz from eight pegmatite fields and provinces worldwide. The NYF and LCT pegmatite families are based on the classification by Černý (1991). The DPA-1, DPA-2 and RMG-1 pegmatite groupings follow the classification of Wise et al. (2021). Black and colored circles indicate averages and outliers, respectively.

pegmatites; however, the concentration overlap is broad, which does not allow for a clear distinction to be made between pegmatite types. The Borborema pegmatites contain quartz with distinctly higher Ti content than the other LCT/ DPA-1/RMG-1 pegmatites.

Except for samples from Hagendorf-Pleystein and San Luis, Al and Li concentrations in quartz show strong positive correlations (Fig. 4B). For the well-correlated samples, the Li and Al contents of quartz do not exceed the Li/Al ratio line of 1:3.89, which corresponds to an atomic ratio of Li to Al of 1:1. NYF/DPA-2 quartz generally has lower Li than LCT/ DPA-1/RMG-1 quartz. However, some LCT/ DPA-1/RMG-1 samples from the Oxford County, Borborema and San Luis, mostly border and wall zone quartz, also contain low Li contents. Germanium, B, Rb and Ga show weak positive correlations with Al (Fig. 4C-F).

In the Ge/Ti versus Al/Ti plot (Fig. 5A), the distinction between NYF/DPA-2 and LCT/ DPA-1/RMG-1 pegmatites is evident, similar to that observed in the Al versus Ti plot (Fig. 4A). The NYF/DPA-2 data plot at the low-ratio end of the Ge/Ti-Al/Ti correlation field, as in the Ge/Ti versus Li plot (Fig. 5B). The distinction between NYF/DPA-2 and LCT/ DPA-1/RMG-1 quartz is, however, not so clear. The data in the Ge/Ti versus Rb are scattered with quartz from Hagendorf-Playstein and Tres Arroyos having the highest Rb concentrations. However, limited data are available for this diagram due to the generally low Rb concentrations (typically <0.9 µgg^{-1}). The quartz data on the Ge/Ti versus B diagram show a very weak positive correlation. However, some quartz analyses from Borborema show high B concentrations.

4.4. *Variability of quartz chemistry among pegmatite fields illustrated as ternary plots*

The Ti - Al/10 - 10*Ge ternary diagram introduced by Schrön et al. (1988) can be used to distinguish quartz of NYF/DPA-2 pegmatites from that of LCT/ DPA-1/RMG-1 pegmatites (Fig. 6A). LCT/ DPA-1/RMG-1

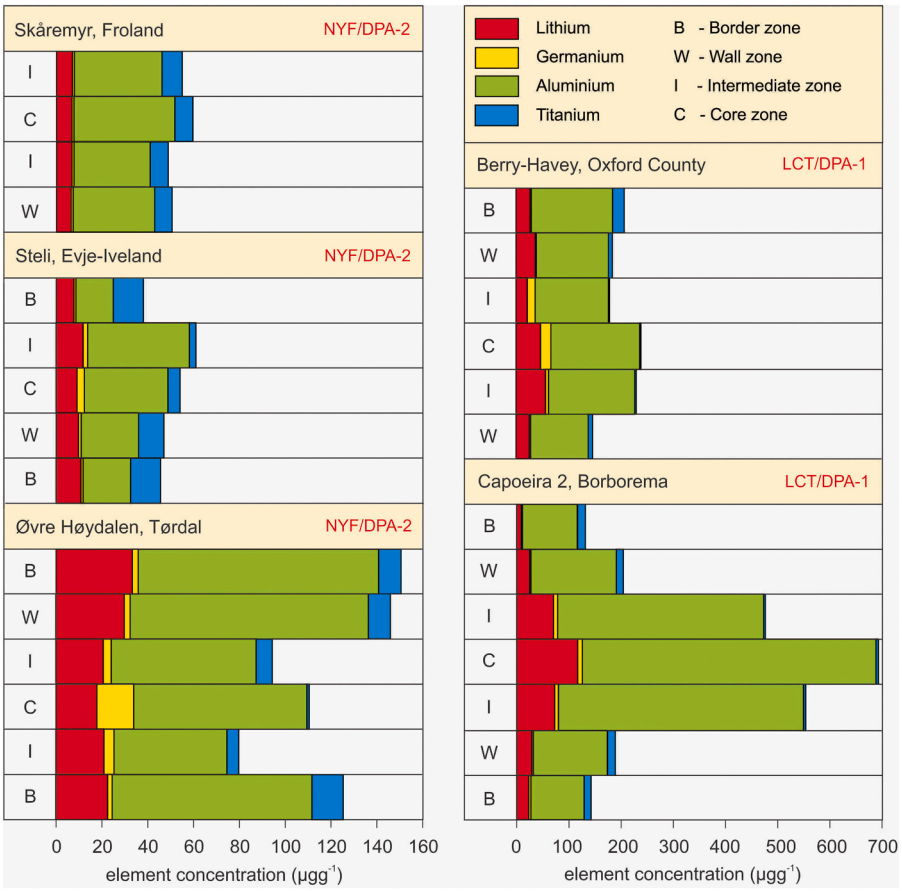

Fig. 3. Internal pegmatite variation of Li, Al, Ge and Ti concentrations in quartz collected along profiles cross-cutting pegmatite bodies. Note the different concentration scales for NYF/DPA-2 (left column) and LCT/DPA-1 (right column) pegmatites. The provided concentrations for individual zones represent average values of two to nine LA-ICP-MS measurements.

quartz plots along the Ge*10 – Al/10 edge and in the center of the diagram, whereas the NYF/DPA-2 quartz plots along the Ge*10 – Ti edge. Only some analyses of the Borborema quartz (LCT/ RMG-1 type) overlap with the NYF/DPA-2 field.

Besides the widely used diagram of Schrön et al. (1988), we introduce the Ti – Al/10 – Rb*50, Ge*10 – Al/10 – Li and Al/10 – Li – Ti ternary diagrams (Figs. 6B-D). Selection of the three elements used in the ternary diagrams is based on empirical handling of the data that helped identify the best combination of elements to be used (see also section on principal component analysis). The Ti – Rb*50 – Al/10 plot differentiates relatively well between NYF/DPA-2 and LCT/ DPA-1/ RMG-1 pegmatites with the exception of Borborema quartz (Fig. 6B). Tres Arroyos, Hagendorf-Pleystein and San Luis quartz plots predominantly along the Al/10 – Rb*50 edge, with Oxford County quartz in the Al/10 corner and the south Norwegian and north Brazilian quartz along the Al/10 – Ti edge towards the Ti corner. In the Ge*10 – Al/10 – Li diagram the Hagendorf-Pleystein quartz plots towards the Al/10 corner, although no strong discrimination can be made amongst the pegmatite types (Fig. 6C). Quartz from Evje-Iveland has proportionally more Li than other south Norwegian quartz (Tørdal and Froland) when plotted on the Al/10 – Li – Ti plot (Fig. 6D). The Hagendorf-Pleystein and San Luis quartz, plotting towards the Al/10 vertex, separate out from the other data. It is worth mentioning that the LCT/ DPA-1/RMG-1 Borborema quartz has the strongest overlap with the Norwegian NYF/DPA-2 quartz in all four ternary diagrams.

4.5. Principal component analysis

Principal component analysis was performed on the dataset to identify covariance between the common elements found in the quartz structure that include Al, Li, Ti, Be, B, Ge and Rb. The remaining elements, Mn, Sr, Na, P, K, Ca and Fe, were excluded from PCA due to their low concentrations in quartz and a lack of any consistent patterns in the dataset. Data for Sb, U, Zn and Ga were only acquired for some of the investigated pegmatite fields and provinces and was not considered in PCA. The data was transformed prior to PCA using centered log-ratio (CLR) transformation in order to address incorrect correlation coefficients resulting from the effects of statistical calculation on raw compositional data (e.g., Aitchison, 1986; Pawlowsky-Glahn et al., 2015). The scaled values (Table 4) show the elements with the largest impact on the variation within the PCs.

Three PCs were determined as significant based on eigenvalues >1 (Fig. 7A; Table 4). PC1 to PC3 account for 70% of the variance within the dataset for CLR-transformed values, with PC1, PC2 and PC3 representing 35%, 20% and 15% of the total variance within the dataset, respectively (Fig. 7A). PC1 is characterized by positive eigenvectors for Al, Li, Ge and B, and negative eigenvectors for Ti, Be and Rb. The high loading scores for Ti (-0.49) and Li (0.49) indicate that these elements have the largest impact on the quartz data variation within PC1. Positive values for Li, Be, B, Ge and Ti, and strong negative values for Rb and Al characterize PC2, with Ge (0.38), Rb (-0.68) and Al (-0.43) accounting for the variation in PC2. PC3 is characterized by high values for Be (0.68) and B (-0.34).

Projections of the PCs onto biplots allow for visual assessment of the quartz data and their regional and group geochemical associations (Figs. 7B-D). For example, quartz from all pegmatites in Norway shows a strong association with Ti and Be. In contrast, quartz from Hagendorf-Pleystein, Tres Arroyos, and to a lesser extent, San Luis, is more

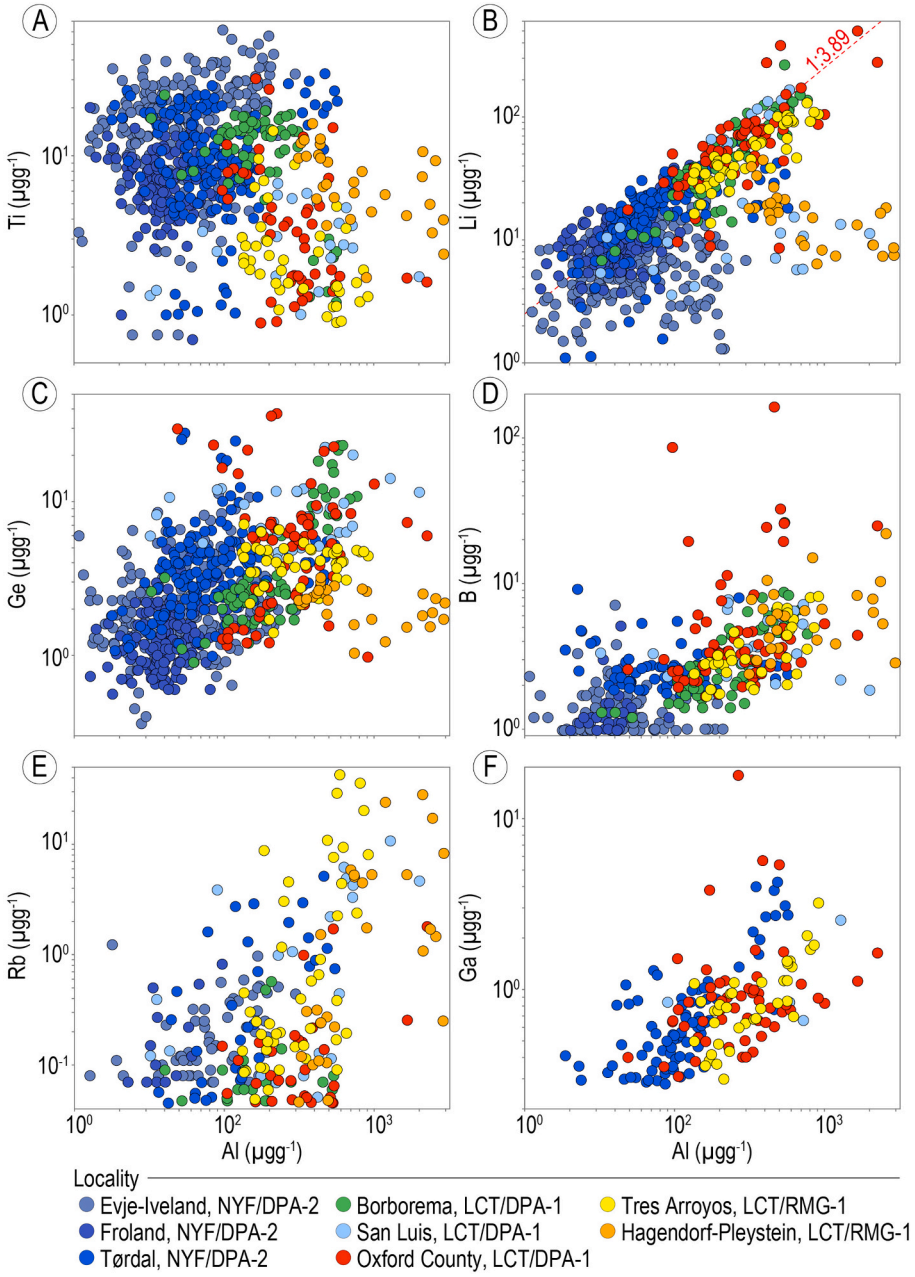

Fig. 4. Binary plots for trace element concentrations in quartz. (A) Al versus Ti; (B) Al versus Li; (C) Al versus Ge; (D) Al versus B; (E) Al versus Rb; (F) Al versus Ga.

strongly affiliated with Rb and Al. Quartz from Oxford County, Borborema and San Luis form a cluster affiliated with Li, B and Ge, although some scatter exists for the latter two localities. When the quartz data are categorized according to pegmatite family, PC1 provides the most information and shows the strong association of quartz from NYF pegmatites with Ti and Be, and that of LCT pegmatites with Li, B, Al, Ge and Rb. Pegmatites categorized according to Wise et al. (2021) shows that PC2 has the most influence on groupings: quartz from DPA-1 pegmatites is associated with Li, B and Ge, quartz from DP-2 pegmatites is associated with Ti and B, and quartz from RMG-1 pegmatites are associated with Rb and Al.

5. Discussion

5.1. Genetic and economic implications of internal pegmatite quartz trace-element variation

The variability of quartz chemistry within a single pegmatite body relative to an entire pegmatite field was used to test the robustness of quartz trace-element content as a genetic and exploration pathfinder (Fig. 8). The range of Ti (1 to 13 µgg^{-1}) and Al (39 to 128 µgg^{-1}) concentrations in quartz from the Øvre Høydalen pegmatite spans the lower third of the entire Al and Ti content range (1 to 33 µgg^{-1} and 18 to 547 µgg^{-1}, respectively) of the pegmatite field (Fig. 8A). Quartz from four chemically evolved Tørdal pegmatites is particularly rich in Al with concentrations ranging from 270 to 547 µgg^{-1}. The spread of the Li contents superimposes nearly the entire Li variation of the pegmatite field (Fig. 8B). The data, i.e., high Li and low Ti, confirm mineralogical observations that the Øvre Høydalen pegmatite represents one of the

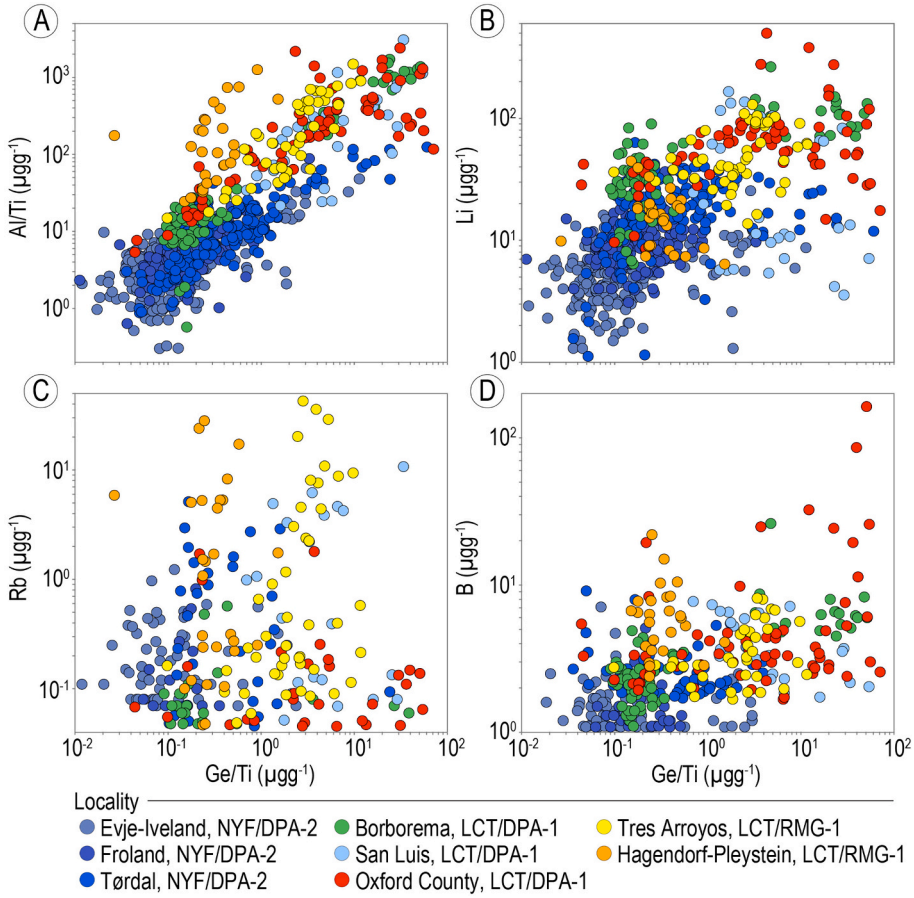

Fig. 5. Binary plots for trace element concentrations in quartz. (A) Ge/Ti versus Al/Ti; (B) Ge/Ti versus Li; (C) Ge/Ti versus Rb; (D) Ge/Ti versus B.

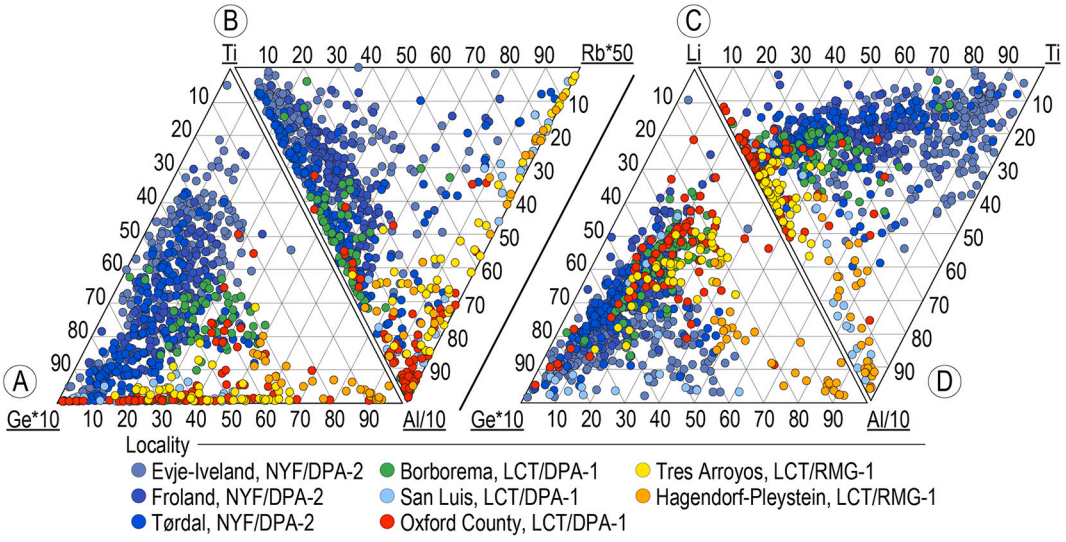

Fig. 6. Ternary plots of trace element distribution in pegmatite quartz.

more fractionated pegmatites within the pegmatite field. It has been shown that high Li in igneous quartz reflects high Li contents in the melt (Breiter et al., 2014; Müller et al., 2015). Frigo et al. (2016) proved through experimental study that Li in quartz increases with the Li saturation of the melt by determining partition coefficients of Li between quartz and silicate melt in spodumene-doped granitic systems. Low Ti in quartz indicates relatively low crystallization temperatures (e.g., Wark and Watson, 2006; Huang and Audétat, 2012). However, the border and wall zones of the pegmatite have primitive quartz compositions indistinguishable from less fractionated pegmatites of the Tørdal field.

Concentrations of Al, Ti and Li in quartz of the Capoeira 2 pegmatite cover roughly the variation of the entire Borborema pegmatite field (Figs. 8C, D). The Capoeira 2 pegmatite is one of the most fractionated pegmatites within the field. Nevertheless, quartz from the border zone

Table 4
Results of PCA on the studied dataset (n = 806 data points) provided as eigenvalues for PC1 to PC7 calculated from CLR-transformed values, with element coordinates (loadings) as displayed in projections illustrated in Figs. 7 and 9.

Eigenvalues for PC1 to PC7							
Eigenvalues	PC1	PC2	PC3	PC4	PC5	PC6	PC7
λ	**2.44**	**1.45**	**1.06**	0.83	0.73	0.51	0.00
λ%	34.78	20.70	15.09	11.85	10.36	7.22	0.00
∑λ%	34.78	55.48	70.57	82.42	92.78	100.00	100.00
Eigenvectors for elements for PC1 to PC7							
Elements	PC1	PC2	PC3	PC4	PC5	PC6	PC7
Li	**0.49**	0.12	0.20	0.22	0.37	0.64	0.33
Be	-0.28	0.28	**0.68**	-0.21	-0.47	0.13	0.31
B	0.37	0.09	-0.34	-0.78	-0.11	-0.03	0.31
Ge	0.35	0.38	-0.26	0.51	-0.49	-0.30	0.29
Rb	-0.25	**-0.68**	-0.26	0.14	-0.29	0.27	0.48
Ti	**-0.49**	0.34	-0.18	0.04	0.51	-0.22	0.55
Al	0.35	**-0.43**	**0.46**	0.01	0.22	-0.60	0.28

Eigenvalues in bold indicate values >1.00 (PC1-PC3) that account for 70% of variance within the dataset.
Eigenvectors in bold indicate the highest loading values and high correlation of an element with its respective PC.

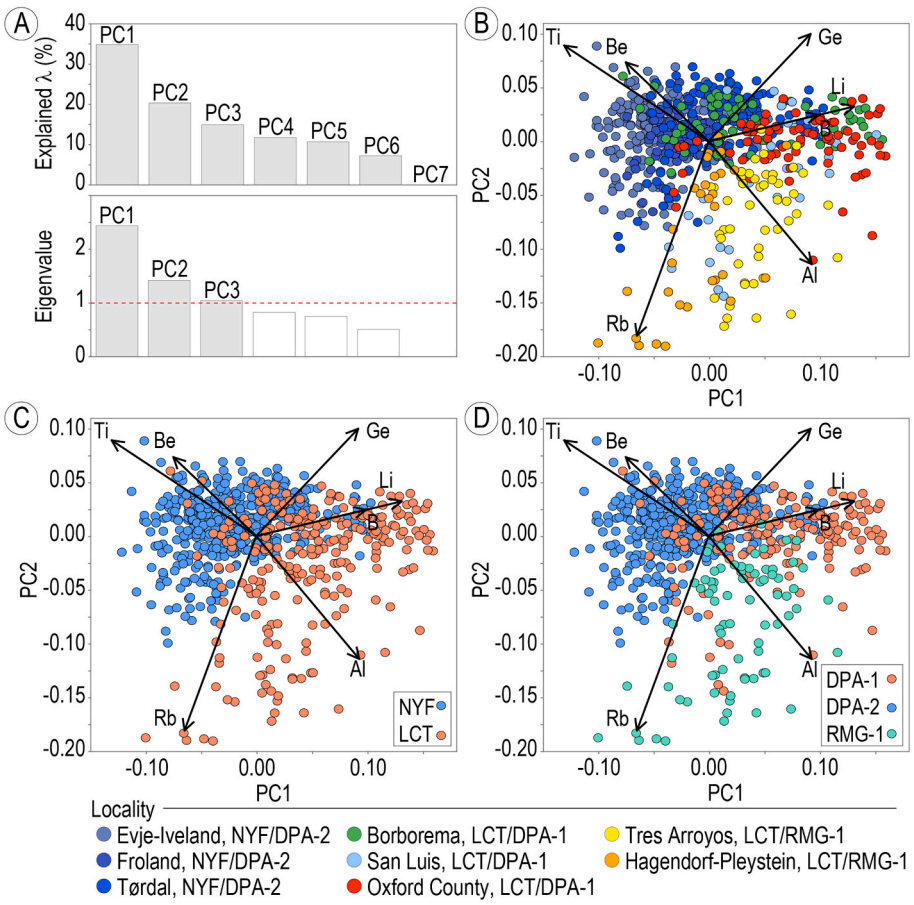

Fig. 7. Principal component analysis results of LA-ICP-MS data for pegmatite quartz. (A) Ranking of eigenvectors by decreasing eigenvalues. Eigenvalues >1 (PC1-3) are statistically relevant. PC3, although statistically little relevant, does not improve regional or genetic discriminations, which are already visible in the binary plots. (B-D) Score plots of the PC1 and PC2 for trace element contents in pegmatite quartz by location (B), NYF and LCT families (C) and DPA-1, DPA-2 and RMG-1 groups (D).

has very primitive compositions (high Ti, low Ge and Li), similar to the least fractionated pegmatites of the field suggesting that only quartz chemistry from the intermediate and core zones reflects the final fractionation degree of pegmatite melt. These findings have two important implications. First, melt fractionation of the investigated pegmatites occurred predominantly *in situ* following melt emplacement. Second, only the quartz from the intermediate and core zones is indicative of potential Li, Cs and Ta mineralization. Quartz chemistry from the border and wall zones of primitive and evolved pegmatites of the same pegmatite fields is mostly indistinguishable across the pegmatite field.

5.2. *The robustness of quartz trace-element contents for chemical discrimination and as exploration pathfinders*

The Al-Ti, Al-Li, and Al/Ti-Ge/Ti binary plots effectively distinguish between the major groups of NYF/DPA-2 and LCT/DPA-1/RMG-1 pegmatites with some overlap between the two groups. A threshold of roughly 100 $\mu g g^{-1}$ Al in quartz can be used to distinguish between the two major pegmatite categories. Most quartz from NYF/DPA-2 pegmatites contains <100 $\mu g g^{-1}$ Al, whereas quartz from LCT/DPA-1/RMG-1 pegmatites contains >100 $\mu g g^{-1}$ Al. The reason for this difference might be the Al saturation of the pegmatites. LCT/DPA-1/RMG-1 melts

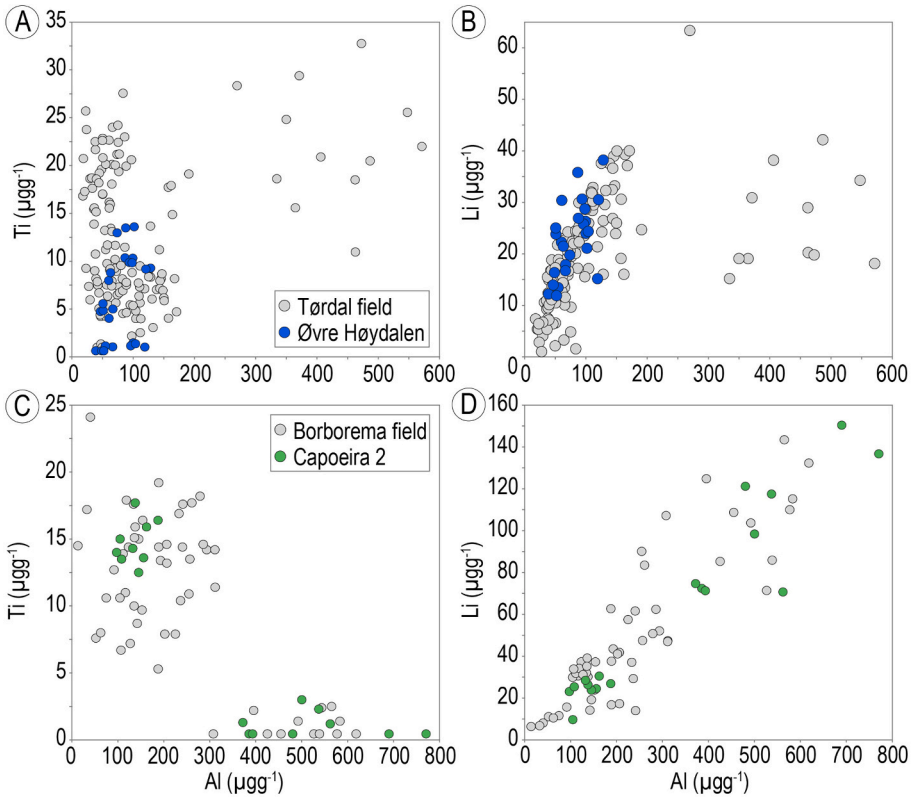

Fig. 8. Variation diagrams of trace elements in quartz from a single pegmatite body relative to the variation within an entire pegmatite field. (A) Al versus Ti and (B) Al versus Li in quartz from the Øvre Høydalen pegmatite (blue dots) relative to the entire Tørdal pegmatite field (grey dots); (C) Al versus Ti and (D) Al versus Li in quartz from the Capoeira 2 pegmatite (green dots) relative to the entire Borborema field (grey dots).

have a higher Al saturation than NYF/DPA-2 melts and quartz growing in highly Al-saturated melts incorporates more Al. Plots of the incompatible elements Ge, B, Rb and Ga (Fig. 4C-F) show weak positive correlations with Al reflecting the fractionation degree of the pegmatite melt but no discrimination between different pegmatite types.

In terms of regional distinction, only the Hagendorf-Pleystein pegmatites separated from the other LCT/DPA-1 samples in the Al-Ge plot (Fig. 4C). The Al-Li and Al/Ti-Ge/Ti are undoubtedly the most suitable plots to illustrate fractionation trends within pegmatite bodies for entire pegmatite fields or worldwide comparison. In this respect, the Borborema pegmatites are the most primitive LCT/DPA-1/RMG-1 pegmatites despite a high bulk B content and being tourmaline-rich. This observation suggests that a high B content does not necessarily imply a high degree of fractionation. Interestingly, quartz from the tourmaline-rich Borborema pegmatites is only moderately enriched in B relative to the high B quartz found in pegmatites from Oxford County. There are two possible reasons for the lower B content in quartz from the Borborema pegmatites compared to that in quartz from the Oxford County pegmatites. First, tourmaline is generally more abundant in the Borborema pegmatites and, thus, B in quartz was probably more effectively buffered by coexisting tourmaline than in the Oxford County pegmatites. Second, tourmaline stability depends not only on the B content in the melt but also on the H_2O activity, oxygen fugacity, temperature and melt composition. Low H_2O activity and high fO_2 increase the stability of tourmaline (Scaillet et al., 1995). At temperatures of 600 °C, tourmaline starts to crystallize with 1 wt.% B_2O_3 in peraluminous melts, whereas ~2 wt.% B_2O_3 is required for crystallization at 750 °C (Wolf and London, 1997). With respect to melt composition, an excess of Al in the melt is needed to produce tourmaline. The presence of F lowers the Al activity in the melt, reducing the stability range of tourmaline (London, 1997; Wolf and London, 1997). Thus, more B is required to crystallize tourmaline in F-richer melts. Because the Borborema pegmatites are less fractionated than those from Oxford County, they have lower H_2O and F and, therefore, crystallized tourmaline from melts with lower B content than those in Oxford County. In this case, the low B content in quartz from the Borobrema pegmatites results from a lower B content in the melts relative to those that crystallized the Oxford County pegmatites. The lower B threshold for gem-quality tourmaline mineralization in the Borborema and Oxford-County quartz is about 5 μgg^{-1}. Quartz from the Hagendorf-Pleystein pegmatites has the highest average B concentrations, yet no tourmaline has been reported in these pegmatites. Thus, B concentrations >5 μgg^{-1} in quartz are not necessarily an indicator for gem-quality tourmaline.

It is evident from the dataset in this study that Li and Ge clearly become enriched in quartz with increasing degree of melt fractionation. However, the Li content in quartz of almost all investigated pegmatites does not exceed the Li:Al = 1:3.89 ratio line, as illustrated in Fig. 4B. Data points above the line are most likely attributable to analytical errors and uncertainties. The corresponding atomic weight ratio given as atoms per formula unit is 1:1. This means that the Al content in quartz controls the maximum uptake of Li in the quartz lattice. This confirms earlier findings that the Li content, which can be incorporated in the quartz lattice, is limited by the substitutional Al content (e.g., Müller and Koch-Müller, 2009). Since Li^+ ions serve as charge compensation for substitutional Al^{3+} defects, Li^+ ions without a coupled Al^{3+} ion do not enter the lattice. This Li buffering mechanism limits the use of Li in quartz to indicate Li-mineralized pegmatites. This has several consequences for the utilization of the Li-in-quartz as a pathfinder for spodumene-montebrasite mineralization. As illustrated in Fig. 9A, pegmatites containing quartz with Li concentrations as low as 5 μgg^{-1} may contain, in rare cases, spodumene and/or montebrasite. However, if the quartz contains >30 μgg^{-1} Li and >100 μgg^{-1} Al, it is relatively certain that the pegmatite also contains Li-rich minerals. Besides high Li and Al, elevated concentrations of B (>2 μgg^{-1}) and Ge (>2 μgg^{-1}) in quartz may

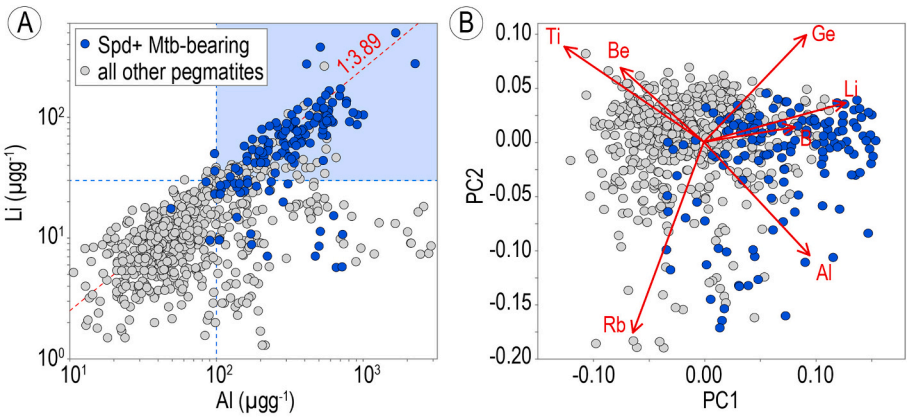

Fig. 9. (A) Al versus Li plot of quartz distinguishing between spodumene/montebrasite-bearing pegmatites (blue dots) and non-spodumene/montebrasite-bearing pegmatites. (B) Binary plot for PC1 and PC2 distinguishing between spodumene/montebrasite-bearing pegmatites (blue dots) and non-spodumene/montebrasite-bearing pegmatites. Only quartz from intermediate and core zones of pegmatites is shown in the figs. The red dashed line in (A) indicates the Al:Li threshold that suggests potential Li mineralization (blue field).

indicate the presence of Li mineralization (Fig. 9B). Beurlen et al. (2014) suggested that Li concentrations in quartz from the core, inner intermediate zones and replacement units exceeding 50 µgg^{-1} could distinguish more evolved spodumene-bearing pegmatites from less fractionated Li-poor pegmatitic bodies. Our results, considering a much broader variety of pegmatites, imply that the Li concentration threshold in quartz indicating Li mineralization can be as low as 30 µgg^{-1}.

Samples from Hagendorf-Pleystein and some from San Luis plot away from the general Al-Li trend (Fig. 4B). In the case of quartz defects, "empty" Li interstitial positions are occupied by other monovalent ions, such as H^+, K^+ or Na^+, or are charge-compensated by coupled P^{5+} (e.g., Müller and Koch-Müller, 2009). Both quartz from Hagendorf-Pleystein and San Luis have the highest average K contents suggesting that Al defects are predominantly charge-compensated by K^+ and Li^+ (Table 3). The Hagendorf-Pleystein pegmatites are relatively poor in Li, which could explain why K was favored over Li. However, the San Luis pegmatites are relatively rich in Li and partially mineralized with spodumene/montebrasite.

In the Ti - Al/10 - 10*Ge diagram according to Schrön et al. (1988), all pegmatite quartz data plot towards the Ge*10 corner. Our data confirm the findings of Schrön et al. (1988), who noticed that pegmatite quartz has elevated Ge concentrations compared to quartz from granites and rhyolites. In addition, our data shows that this diagram distinguishes well between NYF/DPA-2 and LCT/ DPA-1/RMG-1 pegmatites. Quartz from LCT/ DPA-1/RMG-1 pegmatites plots along the Ge*10 – Al/10 edge and in the center of the diagram, whereas the NYF/DPA-2 quartz plots along the Ge*10 – Ti edge. Only some analyses of the Borborema quartz (LCT/ RMG-1) overlap with the NYF/DPA-2 field. In fact, Borborema quartz has the strongest overlap with the Norwegian NYF/DPA-2 quartz in all four ternary diagrams shown in Fig. 6. The reason might be a mixed metasedimentary-metaigneous melt source causing the smearing of the quartz chemistry boundaries.

Chemical purity, simply expressed as the total trace element content, is the most important factor in determining the quality of quartz as a raw material. Of the studied pegmatites, the south Norwegian NYF/DPA-2 pegmatites contain quartz with the lowest total trace-element contents (Table 3; Fig. 10). This suggests that NYF/DPA-2 pegmatites provide the best chemical quality of quartz, although this would need to be confirmed by more studies on NYF/DPA-2 pegmatites. Among the Norwegian pegmatites, the Froland quartz has the lowest total trace-element contents of 93±61 µgg^{-1} (Table 3). Additionally, the Froland pegmatites quartz chemistry is relatively consistent across the pegmatite body, providing a consistent quartz product. As illustrated in Fig. 3, the contrast in quartz chemistry between pegmatite margin (border and wall zone) and core increases with increasing differentiation of the pegmatite-forming melt. This suggests that the most primitive NYF/DPA-2 pegmatites provide the best chemical quality of quartz, not only in terms of low trace-element contents but also in terms of chemical homogeneity. The disadvantage of NYF/DPA-2 pegmatite quartz is the high Ti content relative to LCT/DPA-1/RMG-1 pegmatites. This is caused by generally higher crystallization temperatures of the NYF/DPA-2 pegmatites (e.g., Wark and Watson, 2006; Huang and Audétat, 2012) and by higher Ti saturation of the melts. Our finding is supported by the experimental studies of Frigo et al. (2019) who showed that igneous quartz gets chemically purer with increasing depth of origin. The primitive Froland pegmatites formed at depths >13 km (Müller

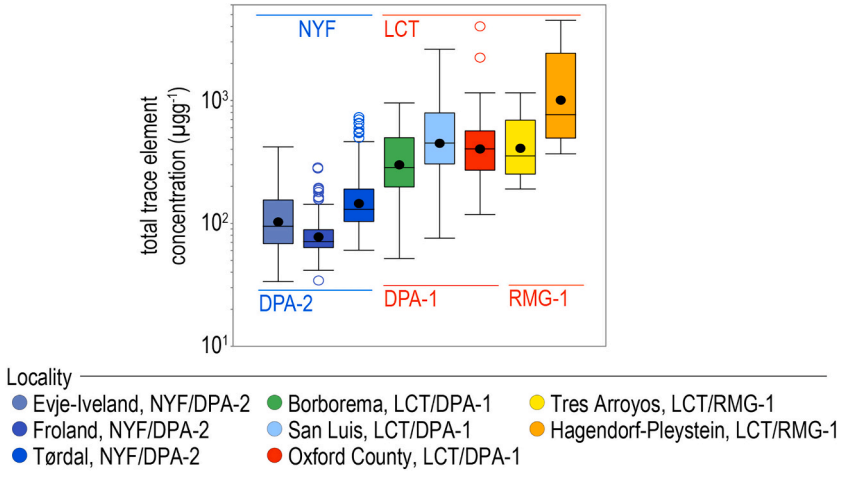

Fig. 10. Box-and-whisker diagram showing the range of the total sum of Al, Li, Ti, Be, B, Ge and Rb in pegmatite quartz from eight pegmatite fields and provinces worldwide. Black and colored circles indicate averages and outliers, respectively.

et al., 2015) and have quartz with lower total trace element contents than that from, for example, the Tres Arroyos pegmatites, which were emplaced at ≤8 km depth and have high total trace element contents in quartz (Garate-Olave et al., 2017). Granite-derived LCT/DPA-1 pegmatites have the highest total trace-element concentrations and are therefore least suitable for high-quality quartz products.

6. Conclusions

Quartz LA-ICP-MS data from 254 pegmatites occurring in eight pegmatite fields and provinces worldwide revealed a wide range of trace-element contents. The variability discriminates chemical and genetic types of pegmatites, and in some cases, the regional origin. Binary diagrams for Al-Ti, Al-Li and Al/Ti-Ge/Ti provide effective discrimination between NYF/DPA-2 and LCT/DPA-1/RMG-1 type pegmatites. Even more effective in discriminating between NYF/DPA-2 and LCT/DPA-1/RMG-1 type pegmatites is the Ti - Al/10 - 10*Ge ternary diagram. Additionally, anatectic DPA-1 and granite-pluton-derived RMG-1 pegmatites can be distinguished by PCA applied to Al, Li, Ti, Be, B, Ge and Rb contents in quartz. The latter are characterized by high Rb and Al concentrations in quartz.

Region-specific characteristics for quartz chemistry include (1) the low Li and Ge and high Al of quartz from the Hagendorf-Pleystein pegmatites and (2) the high Li and Ge and moderate Al of quartz from the Oxford County pegmatites. The results imply that the chemistry of pegmatite quartz is mainly controlled by the origin (source rock chemistry) of pegmatite melt and to a much lesser degree by the geodynamic setting of the pegmatite field and province.

NYF and DPA-2 type pegmatites contain quartz of significantly lower total trace-element contents, which bears important implications from an economic perspective, making it more suitable for high-tech application. However, variation in quartz chemistry across the zones of most of the investigated pegmatite bodies makes the production of a homogeneous quartz product challenging. The most chemically primitive NYF and DPA-2 type pegmatites within pegmatite provinces or pegmatite fields will yield relatively homogenous quartz for production, e.g., the Skåremyr pegmatite of the Froland field.

Systematic quartz sampling from pegmatite intermediate and core zones can establish regional fractionation trends and chemical zoning of pegmatite fields. However, the pegmatite core is rarely exposed in unexplored fields and many pegmatites do not have clearly developed core zones. Thus, it is necessary to consistently sample the intermediate zones of exposed pegmatites to establish the regional fractionation pattern of the field.

Pegmatite quartz with >30 $\mu g g^{-1}$ Li and >100 $\mu g g^{-1}$ Al serves as a pathfinder mineral for potential economic Li mineralization. Boron concentrations in quartz >5 $\mu g g^{-1}$ may be utilized as a pathfinder for gem-quality tourmaline mineralization. However, tourmaline mineralization is not developed in all cases where quartz contains >5 $\mu g g^{-1}$, as for example, in the Hagendorf-Pleystein pegmatites.

Declaration of Competing Interest

The authors declare that they have no known competing financial interests or personal relationships that could have appeared to influence the work reported in this paper.

Acknowledgements

The authors are very thankful for the constructive reviews by Roland Stalder and an anonymous reviewer and for the editorial handling of this paper by the editor Karen H. Johannesson. This study is funded by European Commission's Horizon 2020 innovation programme under grant agreement No 869274, project GREENPEG New Exploration Tools for European Pegmatite Green-Tech Resources." The grant ID is consequently EU H2020 GA869274.

Appendix A. Supplementary data

Supplementary data to this article can be found online at https://doi.org/10.1016/j.chemgeo.2021.120507.

References

Aitchison, J., 1986. The Statistical Analysis of Compositional Data. Chapman & Hall, London.
Andersen, O., 1926. Feltspat I: Norges Geologiske Undersøkelse 128a, 1–142 (in Norwegian).
Andersen, O., 1931. Feltspat II. Norges Geologiske Undersøkelse 128b, pp. 1–109 (in Norwegian).
Andersen, T., 1997. Radiogenic isotope systematics of the Herefoss granite, South Norway: An indicator of Sveconorwegian (Grenvillian) crustal evolution in the Baltic Shield. Chem. Geol. 135, 139–158.
Araújo, M.N.C., Vasconcelos, P.M., Silva, F.C.A., Jardim de Sá, E.F., Sá, J.M., 2005. $^{40}Ar/^{39}Ar$ geochronologyof gold mineralization in Brasiliano strike-slip shear zones in the Borborema province. NE Brazil. J. South Amer. Earth Sci. 19, 445–460.
Ashworth, L., Kinnaird, J.A., Nex, P.A.M., Harris, C., Müller, A., 2020. Origin of rare-element-mineralized Damara Belt pegmatites: a geochemical and light stable isotope study. Lithos 372–373, 105655. https://doi.org/10.1016/j.lithos.2020.105655. ISSN: 0024-4937.
Bambauer, H.U., 1961. Spurenelementgehalte und γ-Farbzentren in Quarzen aus Zerrklüften der Schweizer Alpen. Schweiz. Mineral. Petrogr. Mitt. 41, 335–369.
Barth, T.F.W., 1931. Feltspat III. Forekomster i Iveland og Vegusdal i Aust-Agder og herreder i Vest-Agder. In: Norges Geologiske Undersøkelse 128b, pp. 1–170 (in Norwegian).
Barth, T.F.W., 1947. The nickeliferous Iveland-Evje amphibolites and its relation. Norges Geologiske Undersøkelse 168a, 1–71.
Baumgartner, R., Moritz, R., Romer, R., Sallet, R., 2006. Mineralogy and U-Pb geochronology of beryl and columbo-tantalite pegmatites in the Seridó pegmatite district, northeastern Brazil. Can. Mineral. 44, 69–86.
Bergstøl, S., Juve, G., 1988. Scandian ixiolite, pyrochlore and bazzite in granite pegmatite in Tørdal, Telemark, Norway. A contribution to the mineralogy and geochemistry of scandium and tin. Mineral. Petrol. 38, 229–243.
Beurlen, H., Rhede, D., Da Silva, M.R.R., Thomas, R., Guimarães, I.P., 2009. Petrography, geochemistry and chemical electron microprobe U-Pb-Th dating of pegmatitic granites in the Borborema Pegmatite Province, NE-Brazil: a possible source of the rare element granitic pegmatites. Terrae 6, 59–71.
Beurlen, H., Müller, A., Silva, D., Da Silva, M.R.R., 2011. Petrogenetic significance of trace-element data analyzed with LA-ICP-MS in quartz from the Borborema pegmatite province, northeastern Brazil. Min. Mag. 75, 2703–2719.
Beurlen, H., Thomas, R., Da Silva, M.R.R., Müller, A., Rhede, D., Soares, D.R., 2014. Perspectives for Li- and Ta-mineralization in the Borborema Pegmatite Province. NE-Brazil: A review. J. South Amer. Earth Sci. 56, 110–127. https://doi.org/10.1016/j.jsames.2014.08.007. ISSN: 0895-9811.
Bingen, B., Davis, W.J., Hamilton, M.A., Engvik, A.K., Stein, H.J., Skår, Ø., Nordgulen, Ø., 2008. Geochronology of high-grade metamorphism in the Sveconorwegian belt, S. Norway: U-Pb, Th-Pb and Re-Os data. Nor. J. Geol. 88, 13–42.
Bjørlykke, H., 1934. The mineral paragenesis and classification of the granite pegmatites of Iveland, Setesdal, southern Norway. Nor. Geol. Tidsskr. 14, 211–311.
Bjørlykke, H., 1937. The granite pegmatites of southern Norway. Am. Mineral. 22, 241–255.
Blankenburg, H.-J., Götze, J., Schulz, H., 1994. Quarzrohstoffe. Deutscher Verlag für Grundstoffindustrie, Leipzig-Stuttgart (in German).
Bradley, D., Shea, E., Buchwaldt, R., Bowring, S., Benowitz, J., O'Sullivan, P., McCauley, A., 2016. Geochronology and tectonic context of lithium-cesium-tantalum pegmatites in the Appalachians. Can. Mineral. 54, 945–969.
Breiter, K., Ackerman, L., Ďurišová, J., Svojtka, M., Novák, M., 2014. Trace element composition of quartz from different types of pegmatites: a case study from the Moldanubian Zone of the Bohemian Massif (Czech Republic). Mineral. Mag. 78, 703–722. https://doi.org/10.1180/minmag.2014.078.3.17.
Breiter, K., Badanina, E., Ďurišová, J., Dosbaba, M., Syritso, L., 2019. Chemistry of quartz–a new insight into the origin of the Orlovka Ta-Li deposit, Eastern Transbaikalia, Russia. Lithos 348, 105206. https://doi.org/10.1016/j.lithos.2019.105206.
Breiter, B., Ďurišová, J., Dosbaba, M., 2020. Chemical signature of quartz from S- and A-type rare-metal granites – A summary. Ore Geol. Rev. 125, 103674.
Brito Neves, B.B., Fuck, R.A., 2013. Neoproterozoic evolution of the basement of the South-American platform. J. S. Am. Earth Sci. 47, 72–89.
Černý, P., 1991. Fertile granites of Precambrian rare-element pegmatite fields: is geochemistry controlled by tectonic setting or source lithologies? Precambrian Res. 51, 429–468.
Černý, P., Ercit, T.S., 2005. The classification of granitic pegmatites: Can. Mineral. 43, 2005–2026.
Cosca, M.A., Mezger, K., Essene, E.J., 1998. The Baltica-Laurentia connection: Sveconorwegian (Grenvillian) metamorphism, cooling, and unroofing in the Bamble sector, Norway: J. Geol. 106, 539–552.
Dill, H.G., 2015. The Hagendorf-Pleystein Province: the Center of Pegmatites in an Ensialic Orogen. Springer Geology, Berlin, Heidelberg.
Dill, H.G., Gerdes, A., Weber, B., 2007. Cu–Fe–U phosphate mineralization of the Hagendorf–Pleystein pegmatite province, Germany: with special reference to laser-

ablation inductively-coupled plasma mass spectrometry (LA–ICP–MS) of limonite-cored torbernite. Mineral. Mag. 71, 371–387.
Dill, H.G., Weber, B., Gerdes, A., Melcher, F., 2009. The Fe–Mn phosphate aplite "Silbergrube" near Waidhaus, Germany: epithermal phosphate mineralization in the Hagendorf–Pleystein pegmatite province. Mineral. Mag. 72, 1143–1168.
Dill, H.G., Škoda, R., Weber, B., Berner, A., Müller, A., Bakker, R.J., 2012. A newly discovered swarm of shear-zone-hosted Bi-As-Fe-Mg-P-rich aplites and pegmatites in the Hagendorf-Pleystein pegmatite province, southeastern Germany: A step closer to the metamorphic root of pegmatites. Can. Mineral. 50, 943–974. https://doi.org/10.3749/canmin.50.4.943.
Dill, H.G., Skoda, R., Weber, B., Müller, A., Berner, Z.A., Wemmer, K., Balaban, S.-I., 2013. Mineralogical and chemical composition of the Hagendorf-North pegmatite, SE Germany – a monographic study. Neues Jhb. Mineral. Abh 190/3, 281–318. https://doi.org/10.1127/0077-7757/2013/0244.
Flem, B., Müller, A., 2012. In situ analysis of trace elements in quartz using laser ablation inductively coupled plasma mass spectrometry. In: Götze, J., Möckel, R. (Eds.), Quartz: Deposits. Mineralogy and Analytics. Springer Geology, Berlin, Heidelberg, pp. 219–236.
Flem, B., Larsen, R.B., Grimstvedt, A., Mansfeld, J., 2002. In situ analysis of trace elements in quartz by using laser ablation inductively coupled plasma mass spectrometry. Chem. Geol. 182, 237–247.
Frigo, C., Stalder, R., Hauzenberger, C.A., 2016. OH defects in quartz in granitic systems doped with spodumene, tourmaline and/or apatite: experimental investigations at 5–20 kbar. Phys. Chem. Miner. 43, 717–772. https://doi.org/10.1007/s00269-016-0828-3.
Frigo, C., Stalder, R., Ludwig, T., 2019. OH defects in coesite and stishovite during ultrahigh-pressure metamorphism of continental crust. Phys. Chem. Miner. 46, 77–89. https://doi.org/10.1007/s00269-018-0987-5.
Frigstad, O.F., 1999. Amazonittpegmatitter i Iveland-Evje. Bergverksmuseets Skrift 15, 60–73 (in Norwegian).
Gallego-Garrido, M., 1992. Las mineralizaciones de Li asociadas a magmatismo ácido en Extremadura y su encuadre en la Zona Centro-Ibérica. PhD Thesis. Universidad Complutense de Madrid. Spain (in Spanish).
Galliski, M.A., 1992. La Provincia Pegmatítica Pampeana: tipología y distribución de sus principales distritos económicos. Congreso Nacional y I Congreso Latinoamericano de Geología Económica 4, 534–537 (in Spanish).
Galliski, M.A., 1994a. La Provincia Pegmatítica Pampeana: I tipología y distribución de sus distritos económicos. Rev. Asoc. Geol. Argent. 49, 99–112 (in Spanish).
Galliski, M.A., 1994b. La Provincia Pegmatítica Pampeana: II Metalogénesis de sus distritos económicos. Rev. Asoc. Geol. Argent. 49, 113–122 (in Spanish).
Galliski, M.A., 2009. The Pampean Pegmatite Province, Argentina: A review. Contributions of the 4th International Symposium on Granitic Pegmatites, PEG2009, Brazil. Estud. Geol. 19, 30–34.
Galliski, M.A., Linares, E., 1999. New K-Ar muscovite ages from granitic pegmatites of the Pampean Pegmatite Province. II South American Symposium on Isotope Geology, Buenos Aires, Argentina. Anales SEGEMAR 34, 63–67.
Galliski, M.A., Márquez-Zavalía, M.F., 2011. Granitic pegmatites of the San Luis ranges. In: 5th International Symposium on Granitic Pegmatites PEG2011. Field Trip Guidebook, Argentina.
Galliski, M.Á., Márquez-Zavalía, M.F., Pagano, D.S., 2019. Metallogenesis of the Totoral LCT rare-element pegmatite district, San Luis. Argentina: A review. J. South Amer. Earth Sci. 90, 423–439.
Galliski, M.Á., von Quadt, A., Márquez-Zavalía, M.F., 2021. LA-ICP-MS U-Pb columbite ages and trace-element signature from rare-element granitic pegmatites of the Pampean Pegmatite Province, Argentina. Lithos 386, 106001.
Garate-Olave, I., Müller, A., Roda-Robles, E., Gil-Crespo, P.P., Pesquera, A., 2017. Extreme fractionation in a granite-pegmatite system documented by quartz chemistry: The case study of Tres Arroyos (Central Iberian Zone, Spain). Lithos 286-287, 162–174. https://doi.org/10.1016/j.lithos.2017.06.009.
Garate-Olave, I., Roda-Robles, E., Gil-Crespo, P.P., Pesquera, A., Errandonea-Martin, J., 2020. The Tres Arroyos granitic aplite-pegmatite field (Central Iberian Zone, Spain): Petrogenetic constraints from evolution of Nb-Ta-Sn oxides, whole-rock geochemistry and U-Pb geochronology. Minerals 10 (11), 1008. https://doi.org/10.3390/min10111008.
Gerler, T., 1990. Geochemische Untersuchungen an hydrothermalen, metamorphen, granitischen und pegmatitischen Quarzen und deren Flüssigkeitseinschlüssen. PhD thesis. University of Göttingen.
González-Menéndez, L., 1998. Petrología y Geoquímica del Batolito Granítico de Nisa-Alburquerque (Alto Alentejo, Portugal; Extremadura, España). PhD thesis. Universidad de Granada. Spain (in Spanish).
Götze, J., 2009. Chemistry, textures and physical properties of quartz – geological interpretation and technical application. Mineral. Mag. 73, 645–671.
Götze, J., Plötze, M., Graupner, T., Hallbauer, D.K., Bray, C.J., 2004. Trace element incorporation into quartz: a combined study by ICP-MS, electron spin resonance, cathodoluminescence, capillary ion analysis, and gas chromatography. Geochim. Cosmochim. Acta 68, 3741–3759. https://doi.org/10.1016/j.gca.2004.01.003.
Götze, J., Plötze, M., Trautmann, R., 2005. Structure and luminescence characteristics of quartz from pegmatites. Am. Mineral. 90, 13–21.
Gruß, H., 1950. Phosphate aus der Feldspatgrube Hagendorf (Oberpfalz). Der Aufschluss 1 (3), 48.
Henderson, I., Ihlen, P.M., 2004. Emplacement of polygeneration pegmatites in relation to Sveco-Norwegian contractional tectonics: Examples from southern Norway. Precambrian Res. 133, 207–222.
Hong, T., Zhai, M.-G., Xu, X.-W., Li, H., Wu, C., Ma, Y.-C., Niu, L., Ke, Q., Wang, C., 2021. Tourmaline and quartz in the igneous and metamorphic rocks of the Tashisayi granitic batholith, Altyn Tagh, northwestern China: Geochemical variability constraints on metallogenesis. Lithos 400–401, 106358. https://doi.org/10.1016/j.lithos.2021.106358.
Huang, R., Audétat, A., 2012. The titanium-in-quartz (TitaniQ) thermobarometer: a critical examination and re-calibration. Geochim. Cosmochim. Acta 84, 75–89.
Ihlen, P.M., Lynum, R., Henderson, I., Larsen, R.B., 2001. Potensielle ressurser av kvarts- og feldspat-råstoffer på Sørlandet, I: Regional prøvetaking av utvalgte feltspatbrudd i Frolandsområdet: Trondheim, Norway. Norwegian Geol. Surv. Report 2001 (044), 46 p. (in Norwegian).
Ihlen, P.M., Henderson, I., Larsen, R.B., Lynum, R., 2002. Potensielle ressurser av kvarts- og feldspat-råstoffer på Sørlandet, II: Resultater av undersøkelsene i Frolandsområdet i 2001: Trondheim, Norway. Norwegian Geol. Surv. Report 2002 (009), 100 p. (in Norwegian).
Jacamon, F., Larsen, R.B., 2009. Trace element evolution of quartz in the charnockitic Kleivan granite, SW-Norway: the Ge/Ti ratio of quartz as an index of igneous differentiation. Lithos 107, 281–291.
Kats, A., 1962. Hydrogen in alpha quartz. Philips Res. Rep. 17, 133–279.
Larsen, R.B., 2002. The distribution of rare-earth elements in K-feldspars as an indicator of petrogenetic processes in granitic pegmatites: Examples from two pegmatite fields in southern Norway. Can. Mineral. 40, 137–151.
Larsen, R.B., Polvè, M., Juve, G., 2000. Granite pegmatite quartz from Evje-Iveland: Trace element chemistry and implications for the formation of high-purity quartz. Norges Geol. Unders. Bull. 436, 57–65.
Larsen, R.B., Henderson, I., Ihlen, P.M., 2004. Distribution and petrogenetic behaviour of trace elements in granitic pegmatite quartz from South Norway: Contrib. Mineral. Petrol. 147, 615–628.
Linares, E., 1959. Los métodos geocronológicos y algunas edades de minerals de la Argentina, obtenidos por medio de la relación plomo-uranio. Rev. Asoc. Geol. Argent. 14, 181–217.
Ling, X.X., Huyskens, M.H., Li, Q.L., Yin, Q.Z., Werner, R., Liu, Y., Tang, G.Q., Yang, Y.N., Li, X.H., 2017. Monazite RW-1: a homogenous natural reference material for SIMS U-Pb and Th-Pb isotopic analysis. Mineral. Petrol. 111, 163–172.
London, D., 1997. Estimating abundances of volatile and other mobile components in evolved silicic melts through mineral–melt equilibria. J. Petrol. 38, 1691–1706.
López de Luchi, M.G., Hoffmann, A., Siegesmund, S., Wemmer, K., Steenken, A., 2002. Temporal constraints on the polyphaser evolution of the Sierra de San Luis. Preliminary report based on biotite and muscovite cooling ages. In: Cabaleri, N., Linares, E., López de Luchi, M.G., Ostera, H., Panarello, H. (Eds.), 15th Congreso Geológico Argentino, Actas I. Asociación Geológica Argentina, Buenos Aires, pp. 309–315.
Maneta, V., Baker, D.R., 2019. The potential of lithium in alkali feldspars, quartz, and muscovite as a geochemical indicator in the exploration for lithium-rich granitic pegmatites: a case study from the spodumene-rich Moblan pegmatite, Quebec. Canada. J. Geochem. Explor. 205, 106336. https://doi.org/10.1016/j.gexplo.2019.106336.
Monnier, L., Salvi, S., Pochon, A., Melleton, J., Béziat, D., Lach, P., Bailly, L., 2021. Antimony in quartz as a vector to mineralization: A statistical approach from five Variscan Sb occurrences (France). J. Geochem. Explor. 221, 106705. https://doi.org/10.1016/j.gexplo.2020.106705.
Mücke, A., 1981. The parageneses of the phosphate minerals of the Hagendorf pegmatite - a general view. Chem. Erde 40, 217–234.
Müller, A., Koch-Müller, M., 2009. Hydrogen speciation and trace element contents of igneous, hydrothermal and metamorphic quartz from Norway. Mineral. Mag. 73, 569–583. https://doi.org/10.1180/minmag.2009.073.4.569.
Müller, A., Breiter, K., Novák, J.K., 1998. 1998. Phosphorus-rich granites and pegmatites of Northern Oberpfalz and Western Bohemia. In: Breiter, K. (Ed.), Genetic Significance of Phosphorus in Fractionated Granites. IGCP Project 373 Correlation, anatomy and magmatic-hydrothermal evolution of ore-bearing felsic igneous systems. Excursion Guide of the International Conference Peršlák, Czech Republic, September 21-24 1998. Czech Geological Survey, Prague, pp. 93–105.
Müller, A., Ihlen, P.M., Kronz, A., 2008. Quartz chemistry in polygeneration Sveconorwegian pegmatites, Froland. Norway. Europ. J. Mineral. 20, 447–463.
Müller, A., Kearsley, A., Spratt, J., Seltmann, R., 2012a. Petrogenetic implications of magmatic garnet in granitic pegmatites from southern Norway. Can. Mineral. 50, 1095–1115. https://doi.org/10.3749/canmin.50.4.1095.
Müller, A., Ihlen, P.M., Snook, B., Larsen, R., Flem, B., Bingen, B., Williamson, B.J., 2015. The chemistry of quartz in granitic pegmatites of southern Norway: Petrogenetic and economic implications. Econ. Geol. 110, 1737–1757. https://doi.org/10.2113/econgeo.110.7.1737.
Müller, A., Romer, R.L., Pedersen, R.-B., 2017. The Sveconorwegian Pegmatite Province – Thousands of pegmatites without parental granites. Can. Mineral. 55, 283–315. https://doi.org/10.3749/canmin.1600075.
Müller, A., Herklotz, G., Giegling, H., 2018. Chemistry of quartz related to the Zinnwald/Cínovec Sn-W-Li greisen-type deposit, Eastern Erzgebirge. Germany. J. Geochem. Expl. 190, 357–373. https://doi.org/10.1016/j.gexplo.2018.04.009.
Nijland, T.G., Harlov, D.E., Andersen, T., 2014. The Bamble sector, south Norway: A review. Geosci. Front. 5, 635–658.
Oftedal, I., 1940. Enrichment of lithium in Norwegian cleavelandite-quartz pegmatites. Nor. Geol. Tidsskr. 20, 193–198.
Pawlowsky-Glahn, V., Egozcue, J.J., Tolosana-Delgado, R., 2015. Modeling and analysis of compositional data. Wiley & Sons, London.
Perny, B., Eberhardt, P., Ramseyer, K., Mullis, J., Pankrath, R., 1992. Microdistribution of Al, Li, and Na in α quartz: Possible causes and correlation with short-lived cathodoluminescence. Am. Mineral. 77, 534–544.
Potrafke, A., Stalder, R., Schmidt, B.C., Ludwig, T., 2019. OH defect contents in quartz in a granitic system at 1-5 kbar. Contrib. Mineral. Petrol. 174, 98. https://doi.org/10.1007/s00410-019-1632-0.

Rosing-Schow, N., Müller, A., Friis, H., 2018. A comparison of the mica chemistry of the pegmatite fields in southern Norway. Can. Mineral. 56, 463–488.
Rosing-Schow, N., Romer, R.L., Müller, A., Corfu, F., Škoda, R., Friis, H., 2021. New insights in the formation of Sveconorwegian pegmatites, southern Norway. Precambr, Res (in review).
Rusk, B., Koenig, A., Lowers, H., 2011. Visualizing trace element distribution in quartz using cathodoluminescence, electron microprobe, and laser ablation-inductively coupled plasma-mass spectrometry. Am. Mineral. 96, 703–708. https://doi.org/10.2138/am.2011.3701 703.
Scaillet, B., Pichavant, M., Roux, J., 1995. Experimental crystallization of leucogranite magmas. J. Petrol. 36, 663–705.
Scherer, E., Münker, C., Mezger, K., 2001. Calibration of the Lu-Hf clock. Science 293, 683–687.
Schrön, W., Schmädicke, E., Thomas, R., Schmidt, W., 1988. Geochemische Untersuchungen an Pegmatitquarzen. Z. Geol. Wiss. 16, 229–244.
Seydoux-Guillaume, A.M., Montel, J.M., Bingen, B., Bosse, V., De Parseval, P., Paquette, J.L., Janots, E., Wirth, R., 2012. Low-temperature alteration of monazite: Fluid mediated coupled dissolution-precipitation, irradiation damage, and disturbance of the U-Pb and Th-Pb chronometers. Chem. Geol. 330–331, 140–158.
Siebel, W., Höhndorf, A., Wendt, I., 1995. Origin of late Variscan granitoids from NE Bavaria, Germany, exemplified by REE and Nd isotope systematics. Chem. Geol. 125, 249–270.
Snook, B., 2014. Towards exploration tools for high purity quartz: an example from the South Norwegian Evje-Iveland pegmatite belt. Ph.D. Thesis, Camborne School of Mines. University of Exeter, England.
Solá, A.R., Williams, I.S., Neiva, A.M.R., Ribeiro, M.L., 2009. U–Th–Pb SHRIMP ages and oxygen isotope composition of zircon from two contrasting late Variscan granitoids, Nisa-Albuquerque batholith, SW Iberian Massif: petrologic and regional implications. Lithos 111, 156–167.
Solar, G.S., Brown, M., 2001. Petrogenesis of migmatites in Maine, USA: Possible source of peraluminous leucogranite in plutons? J. Petrol. 42, 789–823.
Solar, G.S., Tomascak, P.B., 2009. The Sebago pluton and the Sebago Migmatite Domain, Southern Maine: results from new studies. Geol. Soc. America, Northeastern Section Meeting. Field Trip 2, 1–24.
Solar, G.S., Tomascak, P.B., 2016. The migmatite-granite complex of Southern Maine: its structure, petrology, geochemistry, geochronology, and relations to the Sebago Pluton, in: Berry, H.N. IV, West, D.P. Jr. (Eds.), Guidebook for Field Trips Along the Maine Coast from Maquoit Bay to Muscongus Bay. New England Intercolleg. Geol. Conf., Maine Geol. Surv. Publ. 21, 19–42.
Solar, G.S., Tomascak, P.B., Brown, M., 2017. Devonian Granite Melt Transfer in Western Maine: Relations Between Deformation, Metamorphism, Melting and Pluton Emplacement at the Migmatite Front. In: Johnson, B., Eusden, J.D. (Eds.), Guidebook for Field Trips in Western Maine and Northern New Hampshire. New England Intercolleg. Geol. Conf., Bates College, pp. 217–246. https://doi.org/10.26780/2017.001.0013.
Stalder, R., 2021. OH point defects in quartz – a review. Eur. J. Mineral. 33, 145–163. https://doi.org/10.5194/ejm-33-145-2021.
Stalder, R., Potrafke, A., Billström, K., Skogby, H., Meinhold, G., Gögele, C., Berberich, T., 2017. OH defects in quartz as monitor for igneous, metamorphic, and sedimentary processes. Am. Mineral. 102, 1832–1842. https://doi.org/10.2138/am-2017-6107.
Steenken, A., Siegesmund, S., López de Luchi, M., Frei, R., Wemmer, K., 2006. Neoproterozoic to Early Paleozoic events in the Sierra de San Luis: Implications fort he Famatinian geodynamics in the Eastern Sierras Pampeanas (Argentina). J. Geol. Soc. Lond. 163, 965–982. https://doi.org/10.1144/0016-76492005-064.
Strunz, H., 1957. Die Phosphat-Paragenese im Hagendorfer Pegmatit. Der Aufschluss, Sonderband 6, 41–54.
Strunz, H., Forster, A., Tennyson, C., 1975. Die Pegmatite der nördlichen Oberpfalz. In: Strunz, H. (Ed.), Zur Mineralogie und Geologie der Oberpfalz, Der Aufschluss, Sonderheft, 26, pp. 105–116.
Van Schmus, W.R., Brito Neves, B.B., Williams, I.S., Hackspacher, P.C., Fetter, A.H., Dantas, E.L., Babinski, M., 2003. The Seridó Group of NE Brazil, a late Neoproterozoic pre- to syn-collisional basin in West Gondwana: insights from SHRIMP U-Pb detrital zircon ages and Sm-Nd crustal residence (TDM) ages. Precambrian Res. 127, 287–327.
Von Quadt, A, Galliski, M.A., 2011. U-Pb LA-ICPMS columbite ages from the Pampean pegmatite province: Preliminary results. PEG2011 Argentina, Contributions to the 5th International Symposium on Granitic Pegmatites, Asociación Geológica Argentina, Publicación Especial 14, 221-223.
Walenczak, Z., 1969. Geochemistry of minor elements dispersed in quartz (Ge, Al, Ga, Fe, Ti, Li, and Be). In: Archiwum Mineralogiczne, pp. 189–335 (in Polish).
Wark, D.A., Watson, E.B., 2006. TitaniQ: A titanium-in-quartz geothermometer. Contrib. Mineral. Petrol. 152, 743–754.
Webber, K.L., Simmons, W.B., Falster, A.U., Hanson, S.L., 2019. Anatectic pegmatites of the Oxford County pegmatite field, Maine. USA. Can. Mineral. 57, 811–815.
Weil, J.A., 1984. A review of electron spin spectroscopy and its application to the study of paramagnetic defects in crystalline quartz. Phys. Chem. Miner. 10, 149–165.
Weil, J.A., 1993. A review of the EPR spectroscopy of the point defects in α-quartz: the decade 1982-1992. In: Helms, C.R., Deal, B.E. (Eds.), Physics and Chemistry of SiO_2 and the Si-SiO interface. 2. Plenum Press, New York, pp. 131–144.
Wise, M.A., 2013. The discrimination of LCT and NYF granitic pegmatites using mineral chemistry: A pilot study. In: Simmons, W.B., Webber, K.L., Roda-Robles, E., Hanson, S.L., Márquez-Zavalía, Galliski, M.Á. (Eds.), Contributions to the 6th International Symposium on Granitic Pegmatites PEG2013. Attitash, New Hampshire, pp. 156–157. http://pegmatology.uno.edu/news_files/PEG2013_Abstract_Volume.pdf (accessed 4 May 2015).
Wise, M.A., Brown, C.D., 2010. Mineral chemistry, petrology and geochemistry of the Sebago granite-pegmatite system, Southern Maine. USA. J. Geosci. 55, 3–26.
Wise, M.A., Müller, A., Simmons, W.B., 2021. A proposed new mineralogical classification system for granitic pegmatites. Can. Mineral. 59 (in press).
Wolf, M.B., London, D., 1997. Boron in granitic magmas: stability of tourmaline in equilibrium with biotite and cordierite. Contrib. Mineral. Petrol. 130, 12–30.